

TECHNICAL REPORT

construction  
engineering  
research  
laboratory



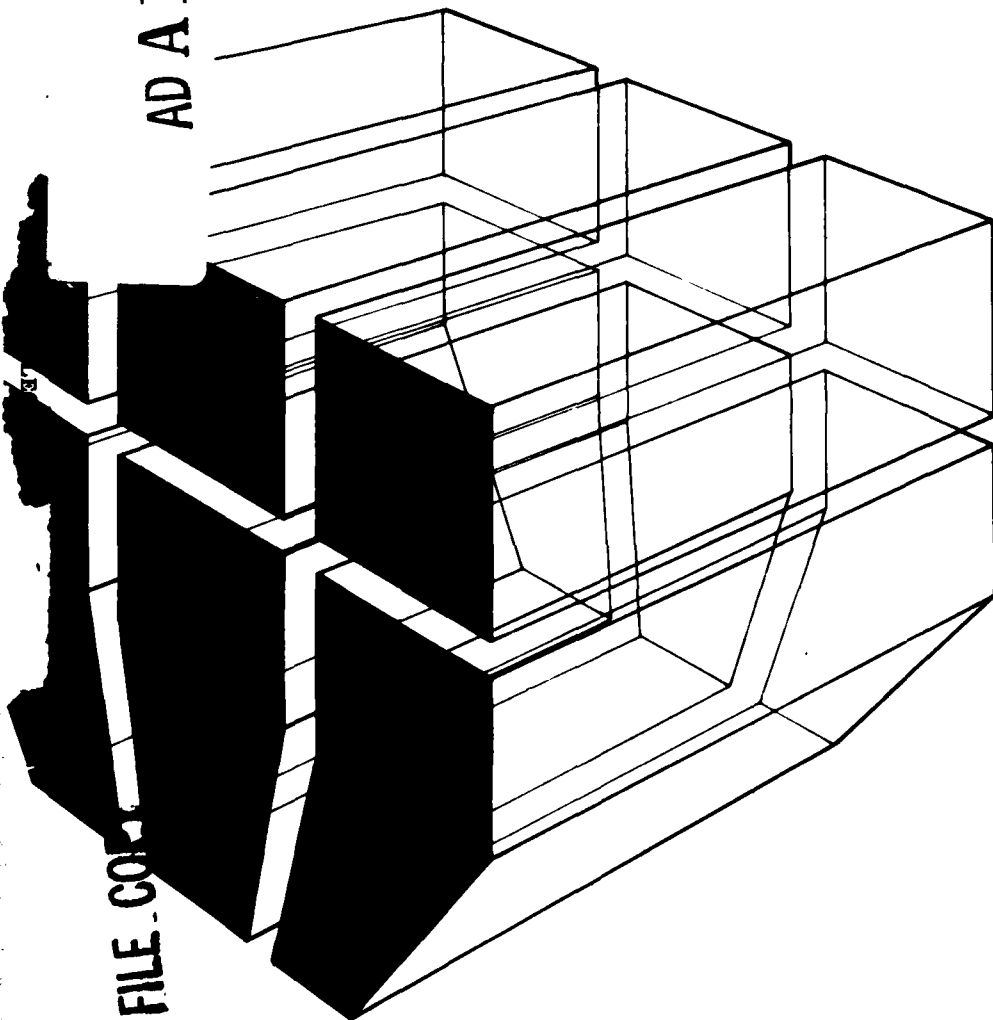
United States Army  
Corps of Engineers  
... Serving the Army  
... Serving the Nation

TECHNICAL REPORT M-292  
September 1981

12

EMP/EMI HARDENING OF ELECTRICAL CONDUIT SYSTEMS

AD A107133



by  
Paul Nielsen

DTIC  
ELECTE  
NOV 10 1981  
A



DTIC FILE COPY

81 11 15

Approved for public release; distribution unlimited.

The contents of this report are not to be used for advertising, publication, or promotional purposes. Citation of trade names does not constitute an official indorsement or approval of the use of such commercial products. The findings of this report are not to be construed as an official Department of the Army position, unless so designated by other authorized documents.

***DESTROY THIS REPORT WHEN IT IS NO LONGER NEEDED  
DO NOT RETURN IT TO THE ORIGINATOR***

UNCLASSIFIED

SECURITY CLASSIFICATION OF THIS PAGE (When Data Entered)

REPORT DOCUMENTATION PAGE		READ INSTRUCTIONS BEFORE COMPLETING FORM
1. REPORT NUMBER CERL-TR-M-292	2. GOVT ACCESSION NO. AD-A107 133	3. RECIPIENT'S CATALOG NUMBER
4. TITLE (and Subtitle) EMP/EMI HARDENING OF ELECTRICAL CONDUIT SYSTEMS.		5. TYPE OF REPORT & PERIOD COVERED
7. AUTHOR(s) Paul/Nielsen		6. PERFORMING ORG. REPORT NUMBER
9. PERFORMING ORGANIZATION NAME AND ADDRESS U.S. ARMY CONSTRUCTION ENGINEERING RESEARCH LABORATORY P.O. Box 4005, Champaign, IL 61820		8. CONTRACT OR GRANT NUMBER(s)
11. CONTROLLING OFFICE NAME AND ADDRESS		10. PROGRAM ELEMENT, PROJECT, TASK AREA & WORK UNIT NUMBERS 4A762719AT40/A1-006
14. MONITORING AGENCY NAME & ADDRESS (if different from Controlling Office)		12. REPORT DATE September 1981
		13. NUMBER OF PAGES 74
		15. SECURITY CLASS. (of this report) Unclassified
		15a. DECLASSIFICATION/DOWNGRADING SCHEDULE
16. DISTRIBUTION STATEMENT (of this Report) Approved for public release; distribution unlimited.		
17. DISTRIBUTION STATEMENT (of the abstract entered in Block 20, if different from Report)		
18. SUPPLEMENTARY NOTES Copies are obtainable from the National Technical Information Service Springfield, VA 22151		
19. KEY WORDS (Continue on reverse side if necessary and identify by block number) electric conduits electromagnetic shielding hardening		
20. ABSTRACT (Continue on reverse side if necessary and identify by block number) Properly designed and installed conduit systems can provide an effective EMP/EMI hardening technique for fixed facility construction. This report presents the results of a CERL study to provide design criteria and to conduct hardness assessments for such shielded systems. Leakage mechanisms are identified, and techniques for determining signal levels coupled to conductors inside conduit systems are presented. EMP shielding properties of conduit hardware items are analyzed and some experimental EMP hardened conduit		

DD FORM 1 JAN 73 1473

EDITION OF 1 NOV 65 IS OBSOLETE

UNCLASSIFIED

SECURITY CLASSIFICATION OF THIS PAGE (When Data Entered)

1475019

sent

UNCLASSIFIED

SECURITY CLASSIFICATION OF THIS PAGE(When Data Entered)

BLOCK 20 CONTINUED

hardware items evaluated. Finally, a number of "in situ" test techniques for identifying and locating EMP-related defects in an installed conduit system are assessed.

UNCLASSIFIED

SECURITY CLASSIFICATION OF THIS PAGE(When Data Entered)

## FOREWORD

This investigation was performed for the Directorate of Military Programs, Office of the Chief of Engineers (OCE), under Project 4A762719AT40, "Mobility, Soils, and Weapons Effects"; Technical Area A, "Weapons Effects and Protective Structures"; Work Unit 006, "EMI Shielding of Conduit Systems." The OCE Technical Monitor was Mr. S. Berkowitz, DAEN-MPE-E.

This investigation was performed by the Engineering and Materials Division (EM), U.S. Army Construction Engineering Research Laboratory (CERL). Dr. R. Quattrone is Chief of EM.

Appreciation is expressed to Dr. W. Croisant, D. Sieber, and R. McCormack for their contributions to this study.

COL L. J. Circeo is Commander and Director of CERL, and Dr. L. R. Shaffer is Technical Director.

Accession For	<input checked="" type="checkbox"/>
NTIS GRA&I	<input type="checkbox"/>
DTIC TAB	<input type="checkbox"/>
Unannounced	
Justification	
Distribution/	
Availability Codes	
Avail and/or	
Special	
A	

## CONTENTS

	<u>Page</u>
DD FORM 1473	
FOREWORD	3
LIST OF TABLES AND FIGURES	5
1 INTRODUCTION.....	9
Background	
Objective	
Approach	
Scope	
Mode of Technology Transfer	
2 EMP HARDENING CHARACTERISTICS OF CONDUIT HARDWARE.....	11
Couplings	
Unions	
Flexible Conduit	
Conduit Bodies and Cast Device Boxes	
Apertures	
3 EMP HARDENED CONDUIT HARDWARE.....	20
4 "IN SITU" CONDUIT SYSTEM TEST TECHNIQUES.....	26
Concept for Detecting Defects by Hall Effect Devices	
S-Band Resonant Cavity	
Standing Wave Defect Location Concept	
5 DIFFUSION CURRENT ANALYSIS.....	39
6 DEFECT LEAKAGE MECHANISM.....	51
EMP Leakage Mechanisms	
Circuit Model for Leakage-Induced Signals	
Coupling Coefficients ( $R_d$ and $M_d$ ) From Flaw Impedances	
7 CONCLUSIONS.....	67
REFERENCES	69
APPENDIX: Example Problems -- Diffusion and Leakage Current Analyses	70
DISTRIBUTION	

## TABLES

<u>Number</u>		<u>Page</u>
1	Values of Equivalent Resistive Coefficient (R) and Inductive Coefficient (M) for Slots Halfway Through 1-In. (25.4-mm) Aluminum Conduit With Center Conductor	17
2	Results of EMP Tests of Unions	23
3	Expansion Union Test Results	23
4	Measurements With FH-302-040 Hall Effect Device, 15 mA Hall Current, 20 A Conduit Current	29
5	Measurements With BH-700 Hall Effect Device, 200 mA Hall Current, 20 A Conduit Current	30
6	Resistivity and Conductivity for Materials Used for Electrical Conduits	42
7	Nominal Dimensions and Parameters of Ferrous Metal and Aluminum Rigid Conduit	42
8	Intermediate Metal Conduit (IMC) Dimensions	44
9	Dimensions of Electrical Metallic Tubing (Thin-Walled Conduit)	45
10	Resistance of Annealed Copper Wire	46
11	Resistance of Rigid Steel Conduit (Ohms per Meter of Length)	47
12	High Frequency Inductance of Wire-Conduit System	49
13	Values of the Polarization of Small Holes in Thin Conducting Sheets	57

## FIGURES

1	Flaw Impedance ( $Z_F$ ) of Typical Coupling	11
2	Flaw Impedance of Conduit Union	13
3	Flaw Impedance ( $Z_F$ ) of 0.015-In. (0.038-mm) Wall Flex-Joint With and Without Copper Strap	14
4	Flaw Impedance ( $Z_F$ ) of 0.03-In. (0.76-mm) Wall Flex-Joint With and Without Copper Strap	14
5	Type C Conduit Body	15

FIGURES (Cont'd)

<u>Number</u>		<u>Page</u>
6	Transverse Slot in Conduit	17
7	Peak Sense-Wire Current Versus Length of Transverse Slot (Width of 0.04 In. [1.0 mm]) in 2-1/2-In. (63.5-mm) Inside Diameter Conduit	18
8	Large Aperture Simulating Completely Eroded Thin-Walled Flexible Conduit Section	18
9	Flaw Impedance ( $Z_F$ ) Versus Frequency For Large Aperture Shown in Figure 8	19
10	Experimental EMP Hardened Union	21
11	Parallel Conduit Transmission Line Configuration	22
12	Machined Conduit Body Cover for EMP Hardening	24
13	"Wrap-Around" Junction Box Cover	25
14	Hall Effect Device	27
15	Magnetic Field Flux Lines Around a Current-Carrying Conduit	27
16	Current Flow on a Conduit With a Defect	27
17	Hall Effect Device Holder	28
18	Grid for Test Locations	28
19	Circuit for Hall Effect Conduit Defect Test Concept	31
20	Resonant Cavity Test Concept	32
21	Resonant Cavity for 1/2-In. (12.7-mm) EMT	33
22	Conduit Defect Location by Standing Waves	35
23	Standing Waves on a Shorted, Two-Conduit Transmission Line	36
24	Standing Wave Defect Location Concept Feasibility Test-Signal With a Defect 10 Ft (3 m) From End	38
25	Standing Wave Defect Location Concept Feasibility Test-Signal With Defect 4 Ft (1.2 m) From End	38
26	Coaxial Conduit-Wire System	47

FIGURES (Cont'd)

<u>Number</u>		<u>Page</u>
27	Peak Amplitude Factor Versus	50
28	Magnetic Field Penetrating Through an Aperture in a Conduit	53
29	Electric Field Penetration Through an Aperture	55
30	Representation of Leakage Sources in a Coaxial Line	56
31	Equivalent Circuit Without Current Source	58
32	Coaxial Transmission Line	61
33	Equivalent Lumped Parameter Circuit	62
34	Buildup of Short-Circuit Current	64

# EMP/EMI HARDENING OF ELECTRICAL CONDUIT SYSTEMS

## 1 INTRODUCTION

### Background

Electromagnetic shielding is often required for Army fixed facilities to protect electronic systems from undesired effects of stray electromagnetic energy. These effects range from false signals causing equipment malfunction to large voltages causing damage to electronic components. Most stray electromagnetic field (electromagnetic interference [EMI]) sources are not intense enough to cause equipment damage; however, such damage is possible from the high current levels expected from nuclear electromagnetic pulse (EMP) effects or the high currents associated with a lightning stroke. Electromagnetic shielding or hardening of a complete facility may be necessary. An effective technique for protecting wiring and cabling in and around a shielded facility is to route that wiring and cabling in a metal conduit system. But commercial conduits and conduit hardware items have not been designed with EMP hardness as a design consideration. In addition, only very limited guidance for such an application of conduit with EMP hardness as a design consideration systems has existed. Therefore, the Office of the Chief of Engineers (OCE) asked the U.S. Army Construction Engineering Research Laboratory (CERL) to establish shielding tests and design criteria for EMP/EMI hardened conduit systems.

CERL's introduction to the problems associated with EMP hardening of conduit systems came during the Safeguard ballistic missile defense (BMD) construction program and consisted of laboratory tests and solution of problems which arose during the construction. Since completing the Safeguard effort, CERL has done more work on developing and evaluating: (1) EMP hardened conduit hardware, (2) EMP hardness test techniques for installed conduit systems, and (3) analytic studies on a procedure for assessing the hardness of conduit systems.<sup>1</sup>

### Objective

The objective of this study was to develop design criteria and shielding tests for EMP/EMI hardened conduit systems.

### Approach

The information in this report is based on laboratory studies and analytical efforts. The study has included (1) experimental determination of EMP signal coupling through conduits and conduit hardware, (2) experimental evaluation of special EMP hardened conduit hardware, (3) development and

<sup>1</sup> W. Croisant, P. Nielsen, D. Sieber, and R. G. McCormack, Development of a Conduit Design Analytical Procedure, Interim Report M-234/ADA056218 (U.S. Army Construction Engineering Research Laboratory [CERL], June 1978).

laboratory feasibility evaluation of test techniques for "in situ" conduit systems, and (4) development of analytic techniques for hardness assessment of conduit systems.

Most of the experimental studies of EMP signal coupling were done with an injected current test technique using a relatively short, fast time pulse developed for the Safeguard work.<sup>2</sup> The test configuration was designed to allow relatively rapid changing of test samples. EMP hardened hardware evaluated included a union designed to allow significant angular displacement, a case-access fitting cover, and a junction box overlapping cover. "In situ" techniques evaluated included: (1) a Hall effect test concept, (2) standing waves on a shorted conduit transmission line, and (3) a clamp-on S-band resonant cavity test technique. The hardness assessment techniques included a diffusion current analysis based on results of laboratory testing and a leakage-current analysis based largely on an analytic approach.

### Scope

The hardness assessment techniques described in this report were designed so that computer operations would not be necessary for their use. Thus, a frequency domain analysis has been avoided since conversion from the frequency domain to the time domain for reconstruction of pulse response can only be done by computer.

### Mode of Technology Transfer

The information in this report will be incorporated into Technical Manual (TM) 5-855-5, Nuclear Electromagnetic Pulse (NEMP) Protection.

<sup>2</sup> W. Croisant, P. Nielsen, D. Sieber, and R. G. McCormack, Development of a Conduit Design Analytical Procedure, Interim Report M-234/ADA056218 (CERL, June 1978), Appendix A.

## 2 EMP HARDENING CHARACTERISTICS OF CONDUIT HARDWARE

The following general analysis of EMP hardening characteristics of conduit hardware is based both on CERL's laboratory studies conducted for the Safeguard BMD system and on later work.

### Couplings

When properly installed, a coupling shields nearly as well as the conduit itself. Therefore, the most important factor affecting leakage through joints is the quality of electrical contact between the mating surfaces of the joints. The flaw impedance (impedance versus frequency) of mated threaded parts is predominantly resistive and nearly independent of frequency below about 10 MHz (Figure 1).<sup>3</sup> The waveshape of an induced voltage is then nearly identical to the waveform of the exciting current. (The flaw impedances of Figure 1, and others, are used later in this report to determine resistive and inductive coupling coefficients [pp 63-65]). When the conduit current is sufficient to induce arcing, the ratio of current on the inner conductor to conduit current is reduced, and the two current waveforms are quite dissimilar. Thus, arcing reduces flaw impedance; however, the arcing threshold is

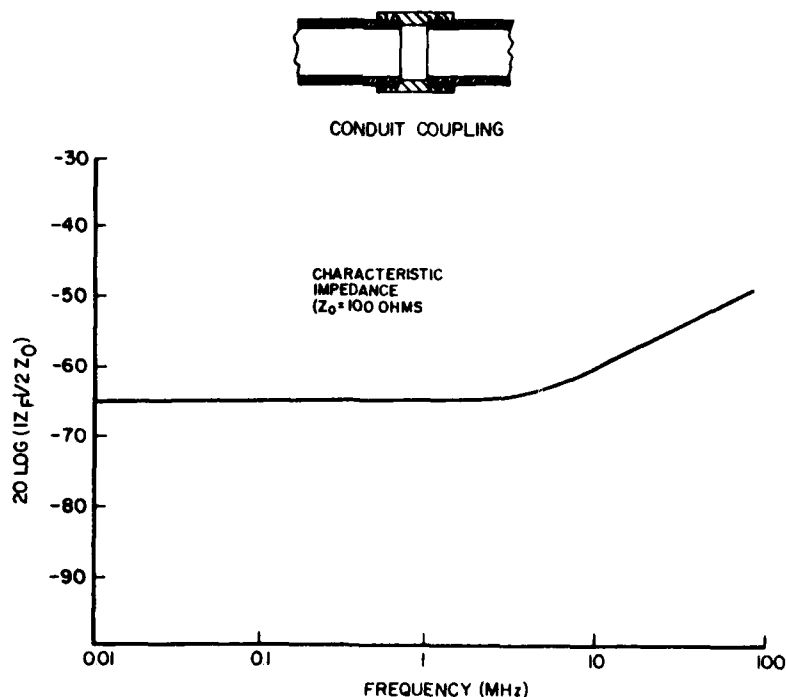


Figure 1. Flaw impedance ( $Z_F$ ) of typical coupling.

<sup>3</sup> The flaw impedance concept was developed by Harry Diamond Laboratories and is reported by H. A. Roberts and J. Capobianco, Safeguard Buried Conduit Studies, HDL-TR-1850 (Harry Diamond Laboratories, September 1978).

impossible to predict. CERL's study failed to show evidence of arcing for a badly rusted coupling (torqued to 300 ft-lbs [42 kg-m]) even when the peak conduit current was increased to 1000 A.

Injected current pulse tests of rusted 1-in. (25.4-mm) conduit-coupling samples indicate that for rusted threads, the tightness of a coupling is not always a good indicator of the EMP condition of the joint. Torque may be related to the resistance of a clean, sound joint. But it is often of little use in determining the resistance of badly rusted threads or couplings, for which a measurement of the direct current resistance is a better indication of the leakage to be predicted. However, any inductive component of flaw impedance will not be indicated by this measurement. The resistance of a joint consisting of heavily rusted conduit threads and a clean, taper-tapped, 1-in. (25.4-mm) coupling was measured and found to be 5.7 milliohms at a torque of 110 ft-lbs (15 kg-m).

Leakage at threads (couplings between conduit sections and connections between conduits and conduit hardware) is almost always a case of poor assembly (e.g., improper tightening, rusted threads).<sup>4</sup> Sections to be joined must be aligned and all threaded connections adequately torqued. Thread leakage can be virtually eliminated with proper assembly precautions.

### Unions

Explosion-proof unions have flat mating surfaces held together by a threaded slip ring (Figure 2). The two halves of the union are threaded to the conduit sections, and the connection is formed by the threaded slip ring. The most important locations for possible leakage for a union are the threads and the slip ring contact.

The flat mating surfaces of clean unions apparently contribute little to the current leakage, and the principal shielding problems occur when the slip ring is in poor contact. Flaw impedances for unions under various test conditions are shown in Figure 2. The flaw impedance can be useful in estimating  $R_d$  and  $M_d$  (coupling coefficients discussed in Chapter 6).  $R_d$  is obtained from the low frequency end of the flaw impedance measurement since  $R_d$  is responsible for most of the low-frequency coupling. Likewise,  $\omega M_d$  can be found from the value of flaw impedance at the high frequency end of the flaw impedance measurement ( $\omega$ , the radian frequency, equals  $2\pi f$ ). The coupling coefficient values cannot account for the irregularities which appear in the measured flaw impedance of unions (Figure 2).

A clean union -- properly aligned and properly installed -- can supply more than 120 dB of shielding; however, a union is less likely than a coupling

<sup>4</sup> D. J. Leverenz, R. G. McCormack, and P. H. Nielsen, EMP Shielding Properties of Conduit Systems and Related Hardware, Technical Report C-19/ADA012729 (CERL, June 1975).

FIVE CASES INVESTIGATED USING A CLEAN UNION CASE I WAS TORQUED TO 50 FT-LBS AND ALL OTHER CASES WERE TORQUED TO 300 FT-LBS

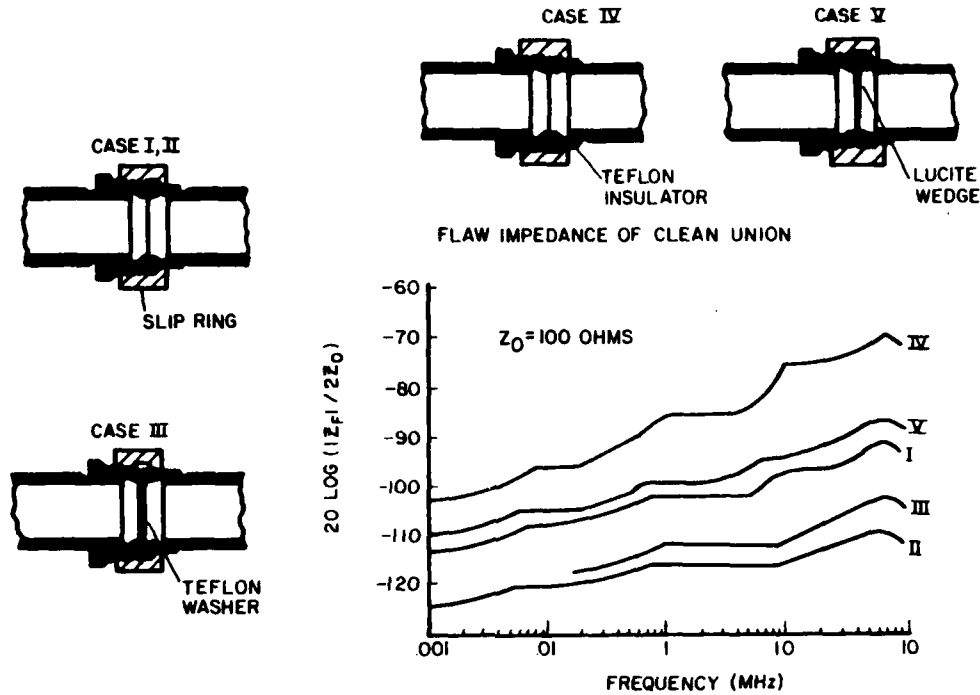


Figure 2. Flaw impedance of conduit union.

to be properly aligned and, therefore, may supply less than adequate shielding.\* Conduit systems should be built so that unions will not have to be used to align or draw together conduit sections. This requires additional care in workmanship and inspection, but the alternative may be specification of expensive, nonstandard hardware.

### Flexible Conduit

If relative movements between the exterior conduits and the shielded structures are expected, flexible connections may be required at exterior walls to accommodate displacements.

Figures 3 and 4 show representative frequency domain flaw impedance for samples of metal bellows flexible conduit used in the Safeguard BMD program. The flaw impedance contributes only to diffusion current;\*\* a comparison of Figures 3 and 4 indicates the influence of material thickness on the frequency domain flaw impedance. The diffusion current can be reduced by incorporating a metal braid over the metal bellows. If the braid is in good electrical contact at each end, it can reduce the overall direct current resistance and

\* "Shielding" as used here is defined as the ratio between maximum amplitudes of the conduit pulse current and the current appearing on a wire inside that conduit without regard to pulse waveshape or  $20 \text{ log } (I_c / I_s)$ , where  $I_c$  equals the conduit current and  $I_s$  equals the current on the internal conductor.

\*\*The diffusion current results from the voltage appearing on the inside of the conduit from the signal propagating or diffusing through the conduit.

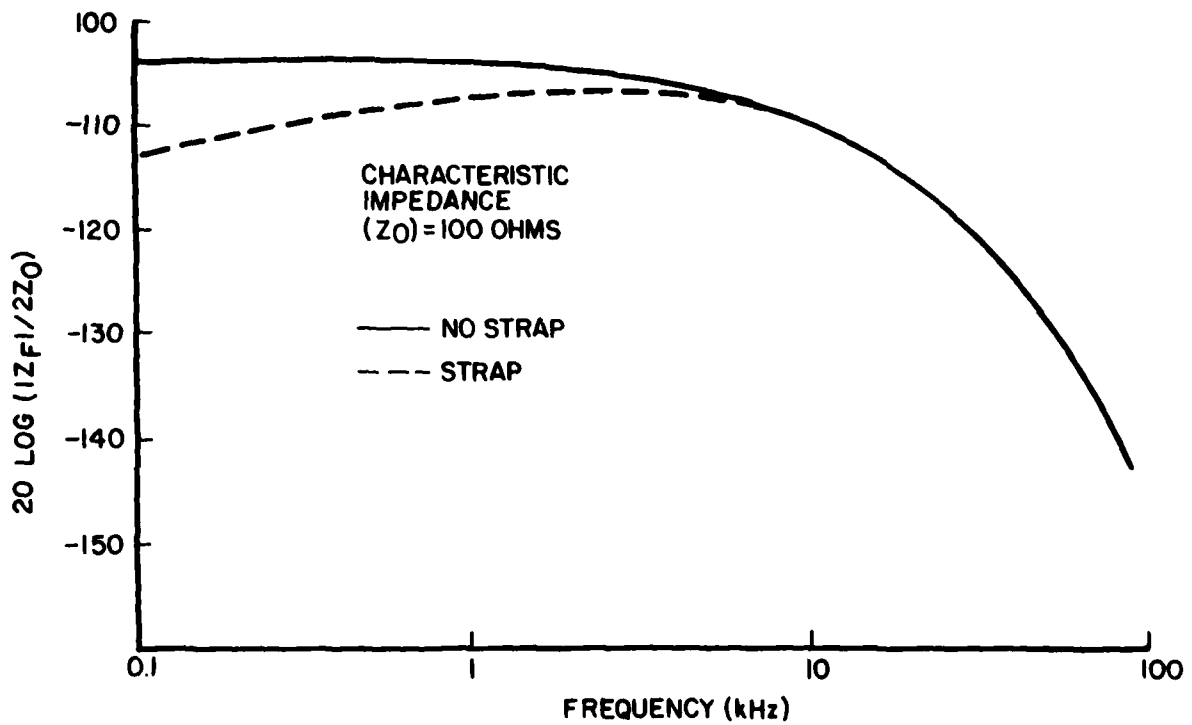


Figure 3. Flaw impedance ( $Z_F$ ) of 0.015-in. (0.038-mm) wall flex-joint with and without copper strap.

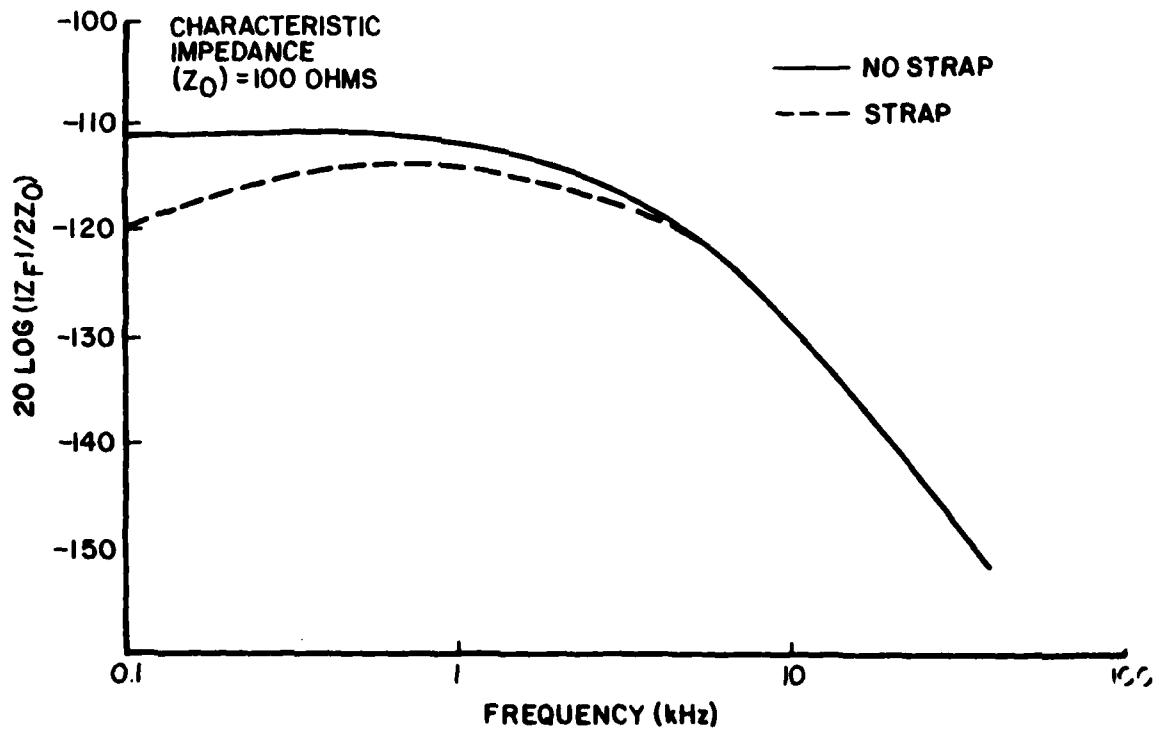


Figure 4. Flaw impedance ( $Z_F$ ) of 0.03-in. (0.76-mm) wall flex-joint with and without copper strap.

increase the equivalent thickness through which the fields must diffuse. Any direct field coupling that might occur through the many small holes in the braid is prevented by the metal bellows. Thus, for maximum EMP hardness, flexible conduit sections should have a wire braid covering and be made with mild steel. Continuous seam bellows must be galvanized inside and outside to prevent corrosion. An alternative approach which may be satisfactory is to use high permeability stainless steel for the flexible conduit. The thin walls of the flexible conduit will also be subjected to a magnetic saturation effect at much lower current levels than the thicker conduit material. This is a nonlinear effect which, at its maximum, results in an effective relative magnetic permeability of 1 for the ferromagnetic material and an accompanying reduction in shielding effectiveness for the material.

#### Conduit Bodies and Cast Device Boxes

A drawing of a Type C, cast-iron conduit body is shown in Figure 5. The cover plates for conduit bodies are often stamped from steel about 1/6-in. (4.2-mm) thick and are attached by two screws (one at each end).

The primary leakage for conduit bodies with good contact at the threaded ends is the gap between the cover and the body. The maximum shielding

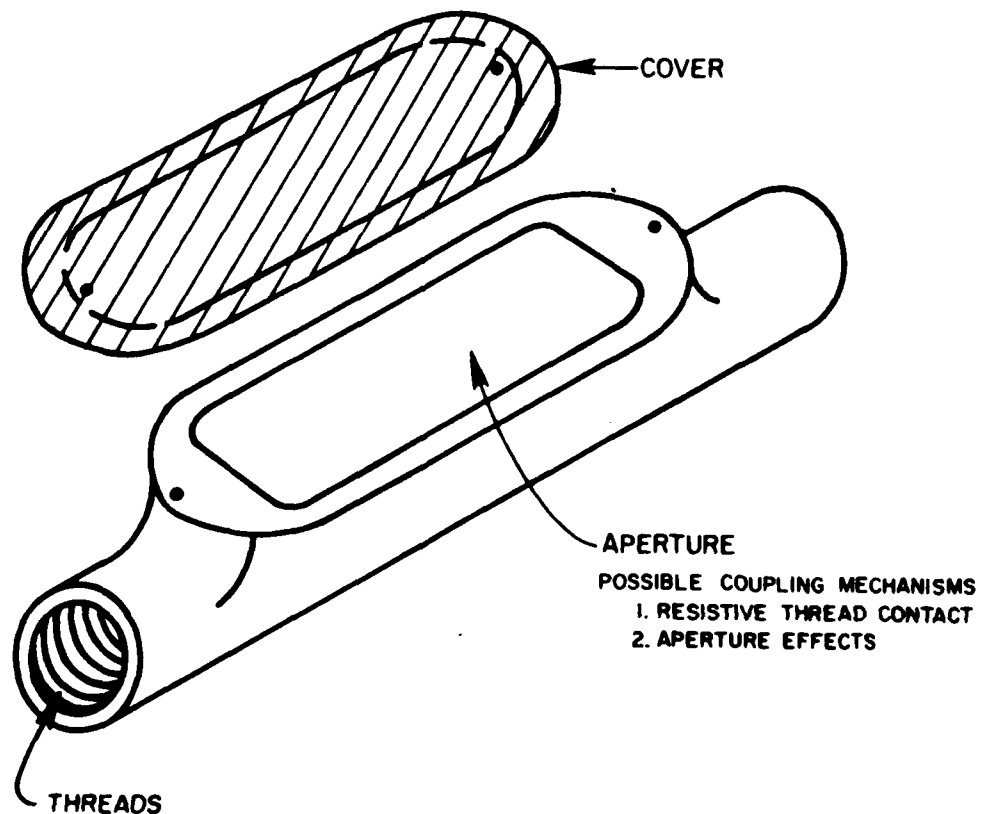


Figure 5. Type C conduit body.

effectiveness would, therefore, be achieved by reducing the gap as much as possible. Tests of radio frequency (rf) interference gaskets (wire mesh, conductive rubber, convoluted wire) for conduit bodies have showed that none of the tested gaskets supplied substantial improvement to shielding effectiveness over the standard cover without a gasket.<sup>5</sup> In addition, if gaskets are used, they must be carefully attached to standard covers to prevent deformation caused by excessive torque on the screws and to assure uniform gasket compression around all edges of the cover.

With no cover, the conduit body presents a sizeable aperture, resulting in extremely high-flux leakage into the conduit with a consequent increase in induced voltage on the internal conductor.

### Apertures

Ideally, no apertures will exist in properly designed EMP hardened conduit systems. The following analysis evaluates potential effects of unintentional apertures that might develop -- e.g., incomplete welding of seams, cracks caused by overtorquing, or holes caused by corrosion. If apertures are suspected, the system could be pressurized to determine the extent of air leakage. Considerable air leakage would indicate a high probability for EMP leakage, although an exact correlation cannot be made.

The magnetic field coupling through apertures depends on the size and shape of the aperture and on the nearness of the internal conductor to the aperture. Compared to a central wire location, resistance coupling resulting from an aperture will not change with wire position; however, inductive coupling for the aperture may be one to two orders of magnitude higher with the conductor near the aperture, or one order of magnitude lower with the conductor opposite the aperture.

Figure 6 shows a transverse slot in a conduit, with Figure 7 illustrating the variation of the leakage signal with transverse circumferential length for constant longitudinal (axial) slot length. The variation is nearly proportional to the cube of the circumferential length.<sup>6</sup>

Table 1 shows the variation of the resistive and inductive coupling coefficients with longitudinal (axial) length for slots cut halfway through a 1-in. (25.4-mm) aluminum conduit (the internal conductor is in the center of the conduit).<sup>7</sup> Coupling coefficients can be used to determine signal coupling levels through apertures; use of these coefficients is described in Chapter 6.

<sup>5</sup> D. J. Leverenz, R. G. McCormack, and P. H. Nielsen, EMP Shielding Properties of Conduit Systems and Related Hardware, Technical Report C-19/ADA012729 (CERL, June 1975).

<sup>6</sup> H. A. Roberts and J. Capobianco, Safeguard Buried Conduit Studies, HDL-TR-1850 (Harry Diamond Laboratories, September 1978).

<sup>7</sup> W. Croisant, P. Nielsen, D. Sieber, and R. G. McCormack, Development of a Conduit Design Analytical Procedure, Interim Report M-234/ADA056218 (U.S. Army Construction Engineering Research Laboratory [CERL], June 1978).

Figure 8 shows a large aperture intended to simulate a completely eroded flexible conduit with only a copper strap remaining. The flaw impedance versus frequency of this configuration is given in Figure 9.

While a small opening in the conduit may not significantly change the transmission line characteristics of the coaxial line formed by the conduit and the inner conductor, large apertures such as the one in Figure 8 may cause an appreciable disruption.

Table 1

Values of Equivalent Resistive Coefficient (R) and Inductive Coefficient (M) for Slots Halfway Through 1-In. (25.4-mm) Aluminum Conduit With Center Conductor

<u>Slot Size, In. (mm)</u>	<u>R, Ohms</u>	<u>M, Henries</u>
0.2 (5)	$5.8 \times 10^{-6}$	$3.04 \times 10^{-10}$
0.39 (10)	$6.36 \times 10^{-6}$	$5.90 \times 10^{-10}$
0.79 (20)	$7.44 \times 10^{-6}$	$8.96 \times 10^{-10}$
1.57 (40)	$1.21 \times 10^{-5}$	$17.1 \times 10^{-10}$
3.15 (80)	$1.80 \times 10^{-5}$	$37.6 \times 10^{-10}$
6.30 (160)	$2.99 \times 10^{-5}$	$63.8 \times 10^{-10}$

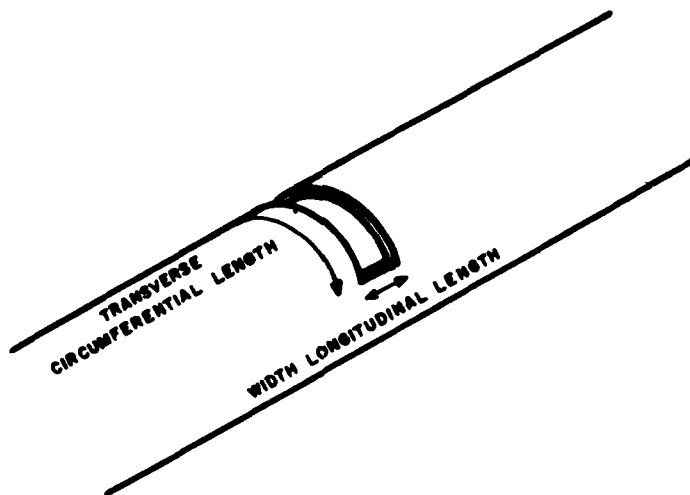


Figure 6. Transverse slot in conduit.

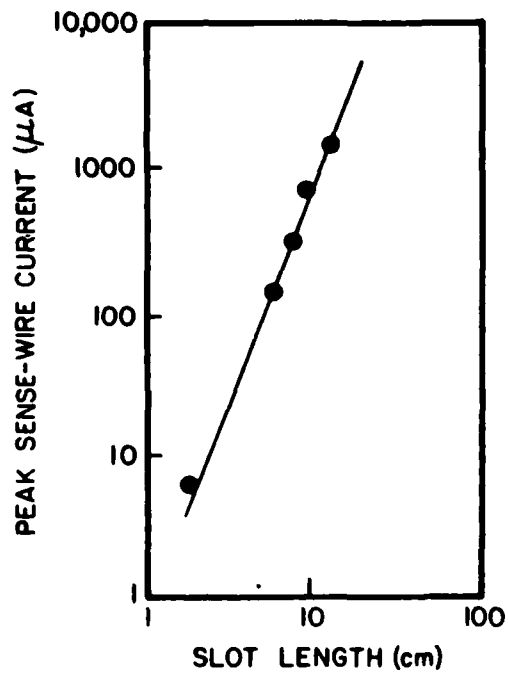


Figure 7. Peak sense-wire current versus length of transverse slot (width of 0.04 in. [1.0 mm]) in 2-1/2-in. (63.5-mm) inside diameter conduit.

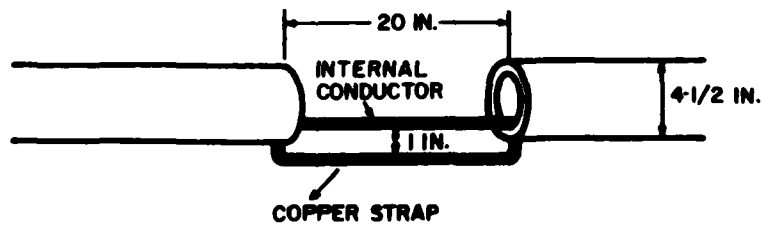


Figure 8. Large aperture simulating completely eroded thin-walled flexible conduit section.

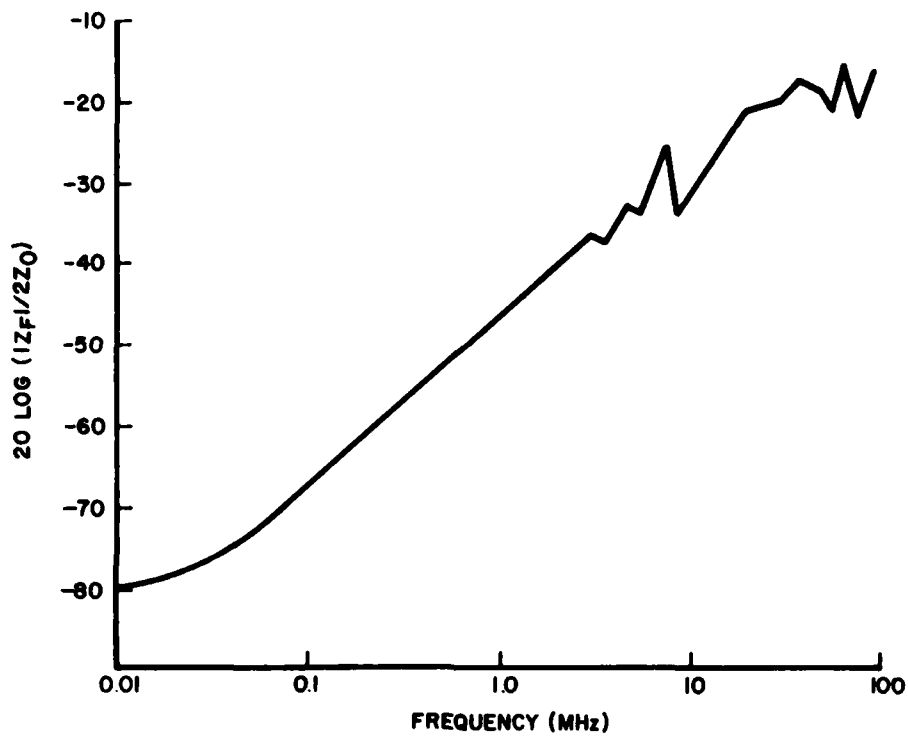


Figure 9. Flaw impedance ( $Z_F$ ) versus frequency for large aperture shown in Figure 8.

### 3 EMP HARDENED CONDUIT HARDWARE

If a leakage signal is to exist on wires within a conduit, it must originate either from a break in the conduit or from some hardware item in the system. Commercial conduit hardware is designed with no consideration for EMP hardness and may or may not provide EMP protection. Specially designed hardware can be expected to be much more expensive, especially for low volume items. However, part of the conduit study program was to design and test such hardware both to determine its desirable characteristics and to see if some slight modifications of commercial items could considerably improve EMP hardness at a relatively minor cost.

Construction of the Safeguard BMD system showed that conduit unions as used presented a problem with EMP hardening. The unions joined sections of preassembled conduit, and length or angular mismatches had to be resolved with the union. In addition, since electrical unions had been identified as having relatively high EMP leakage, they were good candidates for redesign to improve EMP hardness.<sup>8</sup> An experimental union allowing a relatively large tolerance for angular mismatch was designed (Figure 10). One of the basic design criteria determined during the conduit shielding study was that good uniform electrical contact must be maintained between all mating parts. The ball and socket joint provided such contact for the experimental union over a wide range of angular mismatch.

Several different unions were subjected to tests similar to those used at CERL during the Safeguard BMD support tests. The test configuration (Figure 11) consisted of two transmission lines: (1) two parallel conduits which carried the excitation current, and (2) a sensor pickup consisting of one of the conduits which contained the test item and an internal 12-gauge copper wire. Both transmission lines were terminated with resistance matching the characteristic impedance of that transmission line (200 ohms for the excitation current, 100 ohms for the sensor pickup), thus minimizing extraneous reflections. The excitation current was produced by a spark discharge pulser that provided a 200 A pulse with a 10 nanosecond rise time and a 1 microsecond fall time. The sensor pickup instrumentation, an oscilloscope, was located inside a shielded room to reduce electrical noise problems. The peak sensor voltage was measured from an oscilloscope photograph.

The following unions were tested to determine their relative shielding performance:

1. A standard 1-in. (25.4-mm) steel union
2. A 1-in. (25.4-mm) pressure union (liquid tight)
3. A Crouse Hinds "Thredmaker" 1-in. (25.4-mm) union

<sup>8</sup> D. J. Leverenz, R. G. McCormack, P. H. Nielsen, Development and Evaluation of Repairs for EMP Leaks in Conduit Systems, Technical Report C-17/ADA011223 (CERL, April 1975).



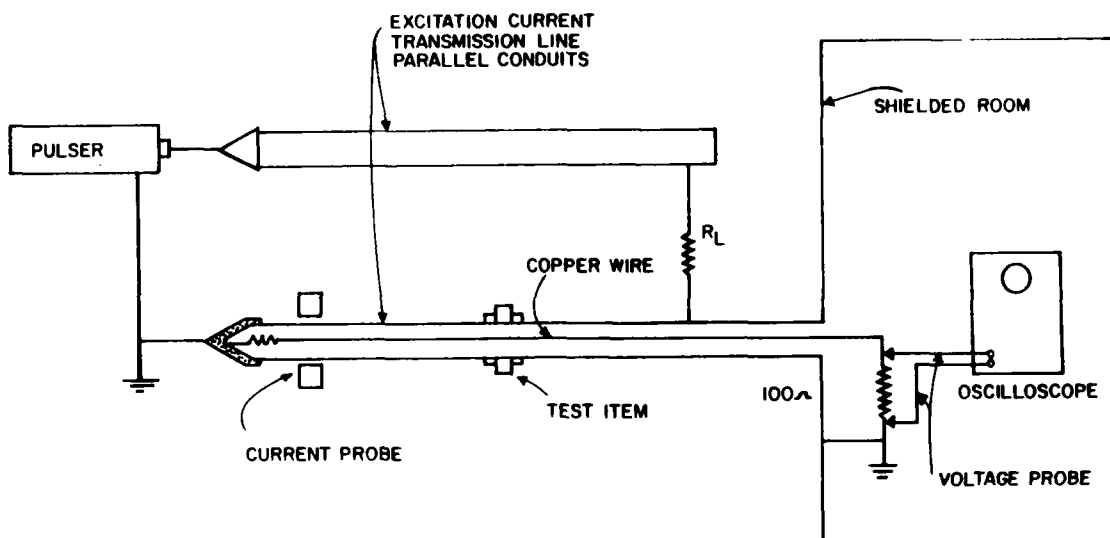


Figure 11. Parallel conduit transmission line configuration.

values of the pulse signal as measured across the 100 ohm terminating resistor inside the shielded room, as shown in Figure 11.

Four conclusions can be drawn from these test results: (1) The pressure union does not present any shielding advantages over the standard electrical union. (2) The "Thredmaker" union appears to have a relatively high leakage under normal assembly conditions. Unless further tests produce more favorable results, this union is not recommended in place of a standard union for EMP hardening requirements. (3) The expansion union also has relatively high leakage and is not recommended for EMP hardened applications. (4) The EMP union provides at least an order of magnitude of increased EMP hardness over a standard electrical union. The rather large size of the union could be decreased with no loss in shielding performance by a reduction in the diameter of the item labeled "coupler" in Figure 10. Additional analysis is necessary to determine the optimum shape of the mating spherical surfaces.

Two additional items designed to provide greater EMP hardening than commercial conduit hardware were a conduit body cover and a wrap-around junction box cover. Neither a conduit body nor a junction box should be used if very large EMP currents are expected on that portion of the conduit system, but both may be used in protected locations.

Conduit bodies are used to provide access to wires inside a conduit. A typical cover is attached by two small screws, one on each end of the cover (Figure 5). Unfortunately, the EMP hardness of the standard commercial configuration is poor. Various covers and gaskets were evaluated during the

Table 2  
Results of EMP Tests of Unions

<u>Union</u>	<u>Peak Voltage With Proper Assembly</u>	<u>Peak Voltage With Angular Offset</u>
Standard	4.8 mV	36 mV
Pressure	4.8 mV, 6.5 mV*	0.46, 0.104 V**
"Thredmaker"	17 mV	19 mV
EMP	+	Less than 1 mV

\*Two tests.  
 \*\*The second value was taken with the union tightened down a quarter turn past the first reading.  
 +No signal detected; minimum detectable signal was about 0.2 to 0.4 mV.

Table 3  
Expansion Union Test Results

<u>Expansion Union</u>	<u>Peak Voltage</u>
Full expanded	10 mV, 12 mV*
1/8 in. (3.22 mm)	25 mV
1/4 in. (6.4 mm) less	36 mV
Half expanded	88 mV
Shortest length	72 mV

\*Two tests.

Safeguard program. The results of these tests were reported earlier.<sup>9</sup> Leakage occurs primarily due to surface resistance between the cover and the fitting wall and flux linkage through the opening left between the cover and the fitting wall. Both of these factors can be reduced significantly by a machined cover and a machined fit inside the fitting housing (Figure 12). For lowest resistance contact, the mating surfaces should be flame sprayed with tin or zinc (soft metals whose surface oxides do not form high resistant contact in a pressure fit). Some increase in EMP/EMI hardness (particularly to radiated signals) can be obtained from a wrap-around junction box cover (Figure 13).<sup>10</sup> Unfortunately, unless cover and boxes are individually machined, individual tolerances are such that significant aperture and resistive leakage will occur.

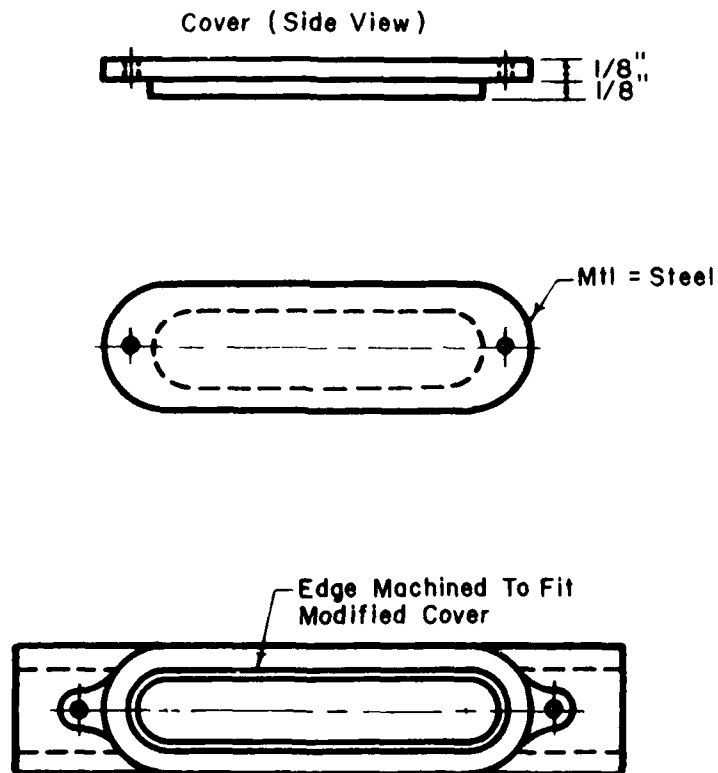


Figure 12. Machined conduit body cover for EMP hardening.

<sup>9</sup> D. J. Leverenz, R. G. McCormack, and P. H. Nielsen, EMP Shielding Properties of Conduit Systems and Related Hardware, Technical Report C-19/ADA012729 (CERL, June 1975), pp 64-71.

<sup>10</sup> D. J. Leverenz, R. G. McCormack, and P. H. Nielsen, EMP Evaluation of Junction Boxes, Junction Box Covers, and Gaskets, Technical Report C-18/ADA010631 (CERL, May 1975).

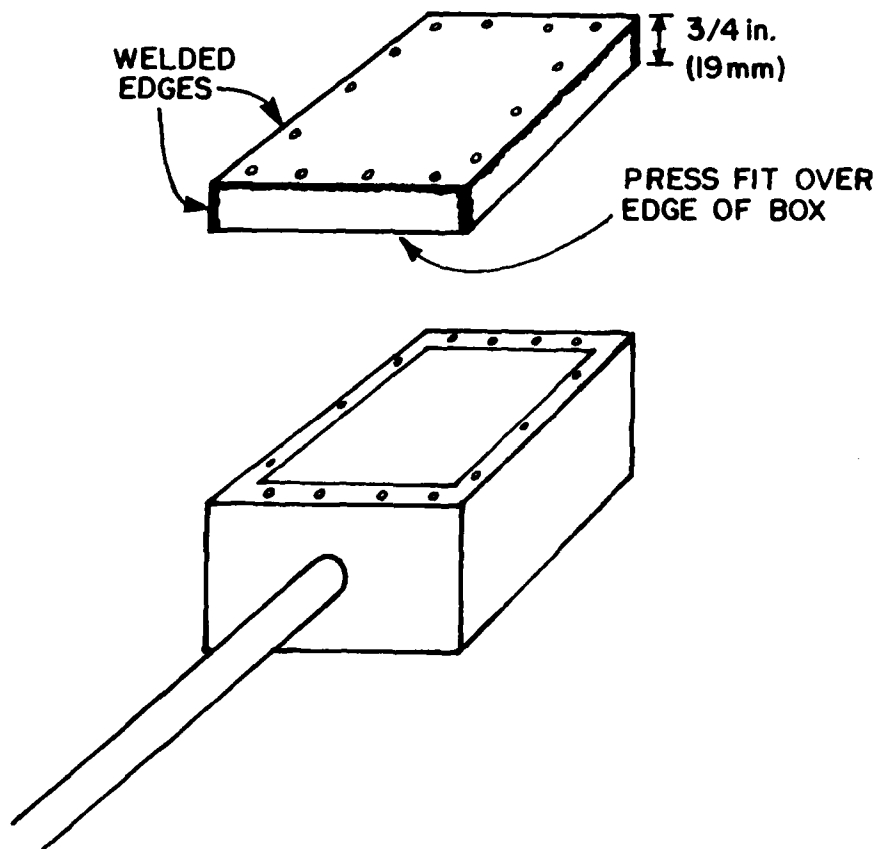


Figure 13. "Wrap-around" junction box cover.

#### 4 "IN SITU" CONDUIT SYSTEM TEST TECHNIQUES

##### Concept for Detecting Defects by Hall Effect Devices

A Hall effect device is a special semiconductor which can be used to detect magnetic fields. If a current flows through the device and the device is immersed in a magnetic field, a voltage proportional to that field will appear on the device perpendicular to both the magnetic field and the direction of current flow (Figure 14). Most practical Hall effect devices are flat plates made of the Hall effect material; each device has two current leads and two voltage leads. The maximum output voltage appears when the magnetic field is perpendicular to the flat surface of the Hall effect device. The excitation current and the magnetic field can be any combination of direct current and alternating current; however, for the test conducted in this study, both were direct current.

Current flow always has an associated magnetic field which can be detected by Hall effect devices. If a current is applied to a uniform conductor, such as defect-free conduit, it will produce a magnetic field with the flux lines being concentric circles around the outside of the conduit (Figure 15). If a defect exists in the conduit, the current flow and the accompanying magnetic field will no longer be uniform (Figure 16). Thus, defects in a conduit can be detected by monitoring the magnetic field around a current-carrying conduit.

CERL used the Hall effect concept to locate defects. A fixture was designed to space 16 devices at equal angles around a conduit and to monitor the output of these devices as they were moved along a current-carrying conduit. A drawing of such a holder is shown in Figure 17. The signal levels from these devices were continuously compared and the defects located. (The comparison also could be done with electronic scanning and a microprocessor.) For the concept feasibility tests described below, only one device was necessary; however, two Hall effect devices of different sensitivities were used for concept evaluation. Two known defects were produced on a 5-ft (1.5-m) section of rigid-steel conduit: (1) A 0.8 in. (20-mm) transverse slot (measured end to end at the external surface of this conduit), and (2) a 1/4-in. (6.3-mm) round hole.

A direct current of 20 A was applied to the conduit. A paper grid with lines every 45 degrees around the conduit and spaced 0.8 in. (20 mm) along the length of the conduit was taped to the conduit with the point (0°, 0) over the center of the defect (Figure 18). The two different Hall effect devices were mounted in the fixture shown in Figure 17. The devices were procured from F. W. Bell, Inc., and were a Model FH-30-040 and a Model BH-700. The mounting fixture consisted of a 1/2-in. (12.7-mm) phenolic piece with a hole large enough to allow it to be slipped along a 1-in. (25.4-mm) conduit. Radial slots were cut at equal angles to allow for the possible mounting of 16 Hall effect devices. The Hall effect voltage was amplified by a 1000x amplifier using a 308a integrated circuit operational amplifier (Figure 19). The amplified voltage was then read on a digital voltmeter. Measurements were made by placing the Hall effect device over a grid location and reading the voltage on the voltmeter. The readings are recorded in Tables 4 and 5 for the FH-302-040 and the BH-700 devices. Considerable direct current level shift was noted

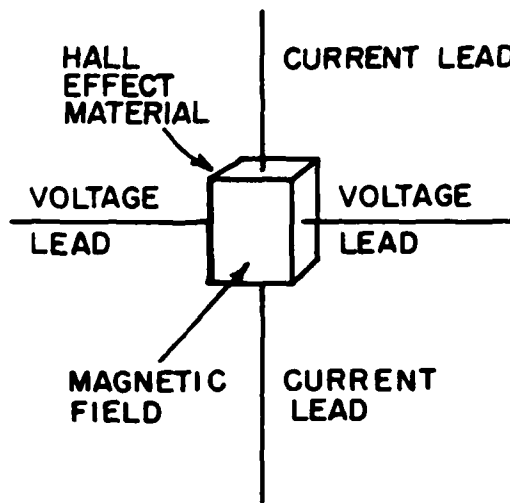


Figure 14. Hall effect device.

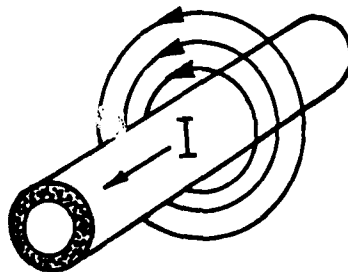


Figure 15. Magnetic field flux lines around a current-carrying conduit.

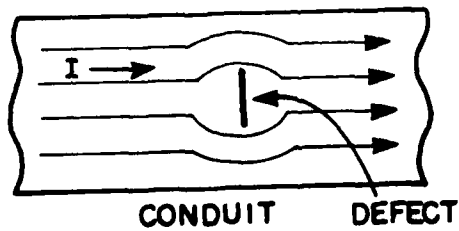


Figure 16. Current flow on a conduit with a defect.

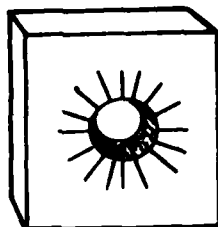


Figure 17. Hall effect device holder.

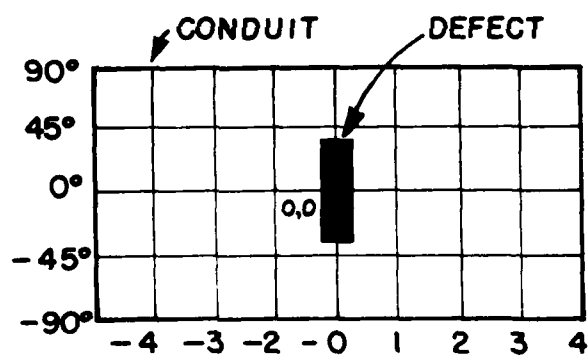


Figure 18. Grid for test locations.

Table 4

Measurements With FH-302-040 Hall Effect Device, 15 mA Hall Current,  
20 A Conduit Current (Values Are in Millivolts)

0.8-In. (20-mm) Slot

	Location									
	-4	-3	-2	-1	0	1	2	3	4	
0	42	40	35	37	35	38	39	42	44	
45 <sup>o</sup>	48	47	47	46	56	51	42	43	47	
90 <sup>o</sup>	50	50	56	54	53	56	52	50	49	
135 <sup>o</sup>	51	51	60	56	48	52	55	55	50	

1/4-In. (6.3-mm) Round Hole

	Location									
	-4	-3	-2	-1	0	1	2	3	4	
0	47	50	47	43	42	42	40	47	52	
45 <sup>o</sup>	50	50	52	50	54	54	54	52	51	
90 <sup>o</sup>	55	57	55	59	59	58	58	56	55	

Table 5

Measurements With BH-700 Hall Effect Device, 200 mA Hall Current,  
20 A Conduit Current (Values Are in Millivolts)

0.8-In. (20-mm) Slot

Location

	-4	-3	-2	-1	0	1	2	3	4
0	135.5	137.0	131.3	134.0	107.3	139.2	136.9	139.2	136.6
45°	132.4	136.9	131.7	142.9	145.4	143.0	126.0	125.9	135.0
90°	137.9	139.8	142.8	133.8	139.8	153.1	139.5	128.6	140.4

1/4-In. (6.3-mm) Round Hole

Location

	-4	-3	-2	-1	0	1	2	3	4
0	138.9	139.0	137.4	132.7	138.8	138.5	135.0	137.6	136.0
45°	139.0	139.0	138.5	136.5	139.0	134.0	139.0	137.9	136.5

No Defect

Location

	-4	-3	-2	-1	0	1	2	3	4
180°	138.5	137.0	135.2	137.3	139.0	136.4	138.5	133.3	149.0
225°	144.2	134.2	135.6	139.6	132.8	140.5	140.4	130.4	132.4

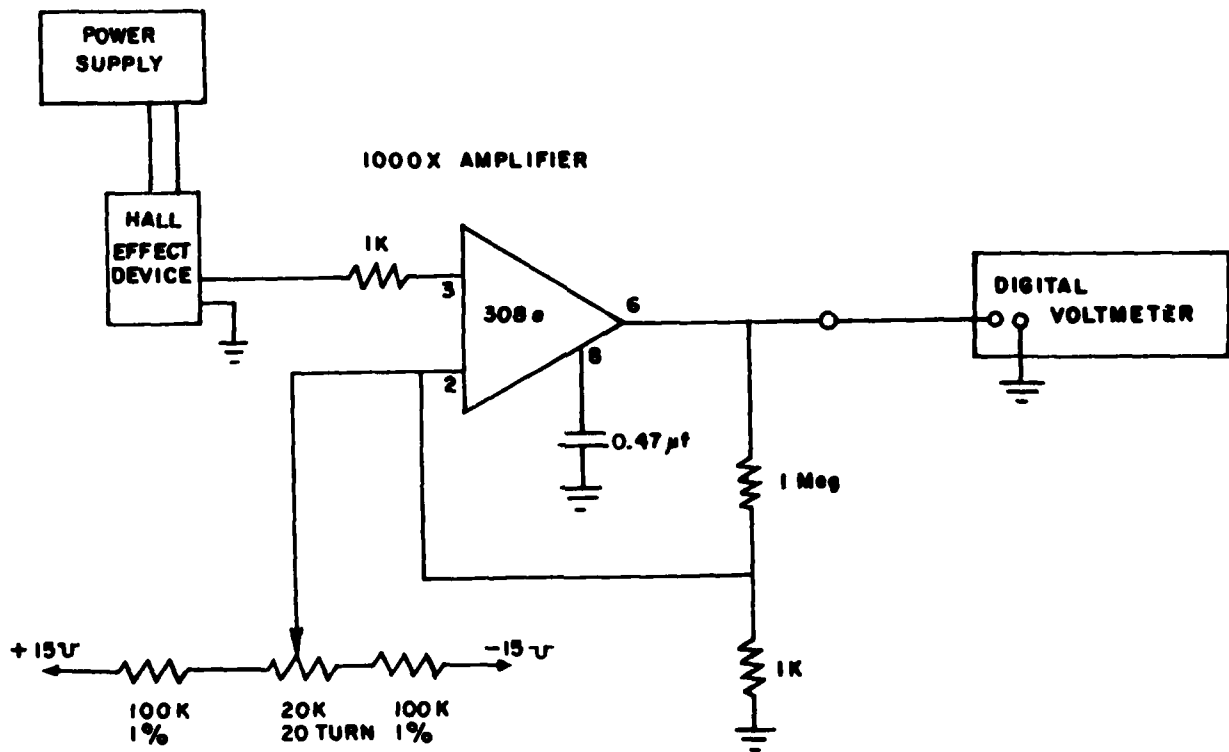


Figure 19. Circuit for Hall effect conduit defect test concept.

during the measurements, and it was found that a significant portion of this variation was due to the degree of heat sinking provided by the conduit for the Hall effect device. The variation was significantly larger for the BH-700 (for which a Hall current of 200 mA was provided), than for the FH-302-040 (which used a Hall current of 15 mA). Much of the variation could be cancelled out by taking a reading of the Hall voltage with no current applied to the conduit and then with 20-A applied. The desired reading is then the difference between these two values. The data shown in Table 5 were taken this way. In addition, some data were taken with no defect present to determine an approximate value for the standard deviation of the data.

From this evaluation, it may be concluded that the defects tested produce a measurable magnetic field variation; however, this variation may be masked by other unrelated factors. The Hall effect devices are very temperature-sensitive, and in the case of the BH-700, a very slight change in the distance from the conduit can cause a significant change in the output due to the heat-sink effects of the conduit. The temperature-related drift problem can be eliminated by exciting the conduit with switched direct current or an alternating current square wave. The change in magnetic field could be measured automatically on a cycle-to-cycle basis, and any device or amplifier drift could be subtracted out.

This technique is probably of limited use for finding defects such as rusty or loose threads or other defects which do not result in a significant disturbance in current flow direction. Breaks or holes, however, should be

very easy to find with this system. The maximum sensitivity for this technique will be limited by signal amplification and noise suppression techniques. For a direct current excitation for the Hall effect device and the 20 A conduit current used, a 1/4-in. (6-mm) hole was readily visible while a 1/8-in. (3-mm) hole was difficult to detect.

### S-Band Resonant Cavity

Electromagnetic shielding leakage can often be detected more readily at microwave frequencies than at some lower frequency. Thus, the concept of illuminating the conduit system in the microwave range and detecting a possible leakage signal within the conduit is suggested. The standard shielding test technique using radiated power from a horn antenna has the disadvantages of high ambient fields necessary for an adequate dynamic range and inefficient use of power. A resonant cavity, however, can have large fields contained within a relatively small controlled volume. The fixture can be designed to open and "clip" onto a conduit at the location of a suspected defect. Leakage can be detected either by an antenna probe placed within the conduit or, for a more general application, by the coaxial system formed by an internal conductor within the conduit. In either case, detection can be done with a sensitive receiver placed where the end of the conduit is accessible. The concept is shown in Figure 20.

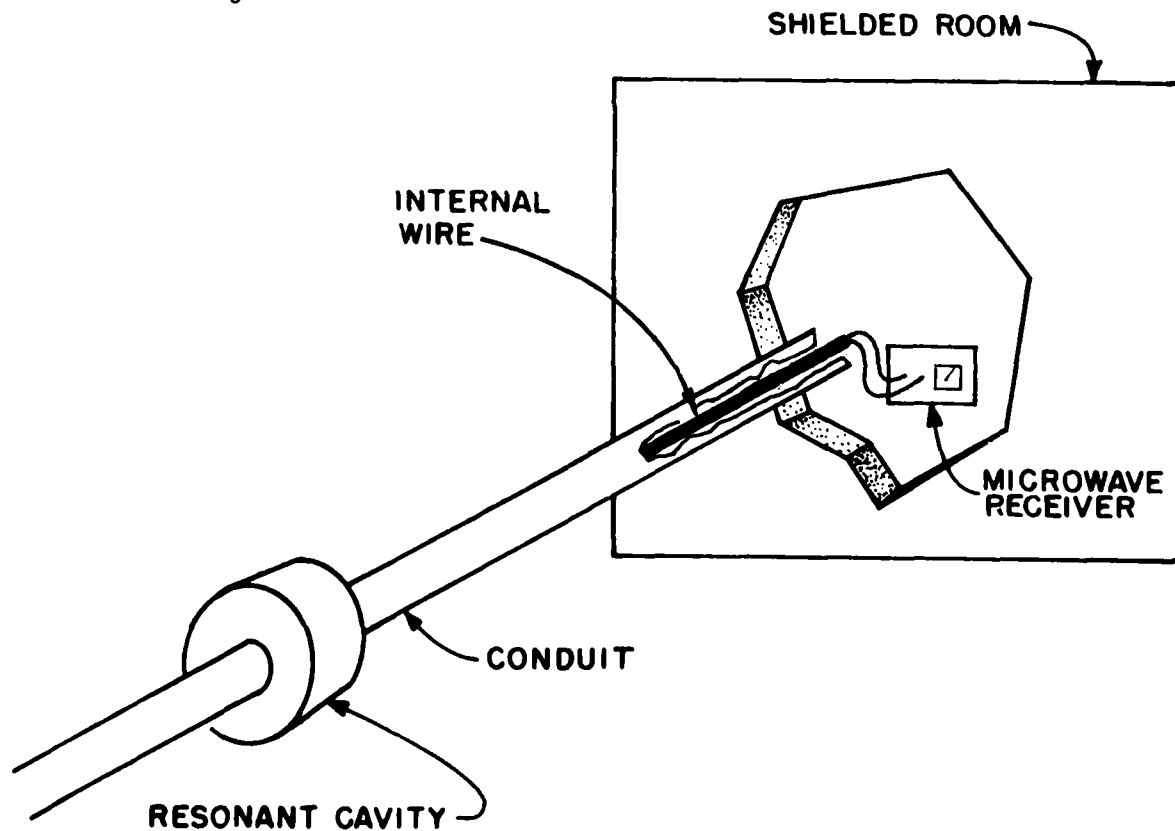


Figure 20. Resonant cavity test concept.

To evaluate the feasibility of this concept, a cavity was designed for use with 1/2-in. (12.7-mm) electrical metallic tubing (EMT), a thin-walled conduit. The 1/2-in. (12.7-mm) dimension was chosen to provide a convenient cavity size for test purposes, and the S-band frequency was picked to ensure a separation of modes within the cavity. The thin-walled conduit was used since its normal couplings and related hardware are pressure fit and do not provide much EMP shielding in their normal installation, thus providing a ready-made test condition. A sketch of the cavity is shown in Figure 21. The finger-stock was used to ensure electrical contact to the conduit. The cavity was excited by applying an input signal to a small loop installed near the outer edge of the cavity. A detecting loop was located 180 degrees opposite the feed loop. The following equipment was used for the test: a Hewlett Packard 616A signal generator for the signal source, with a maximum output of 1 mW; a Tektronix 491 spectrum analyzer for resonance determination, and a Stoddard NM-65T microwave receiver for measurement of the leakage signal. Two 10-ft (3-m) sections of conduit were jointed with a coupling for this test.

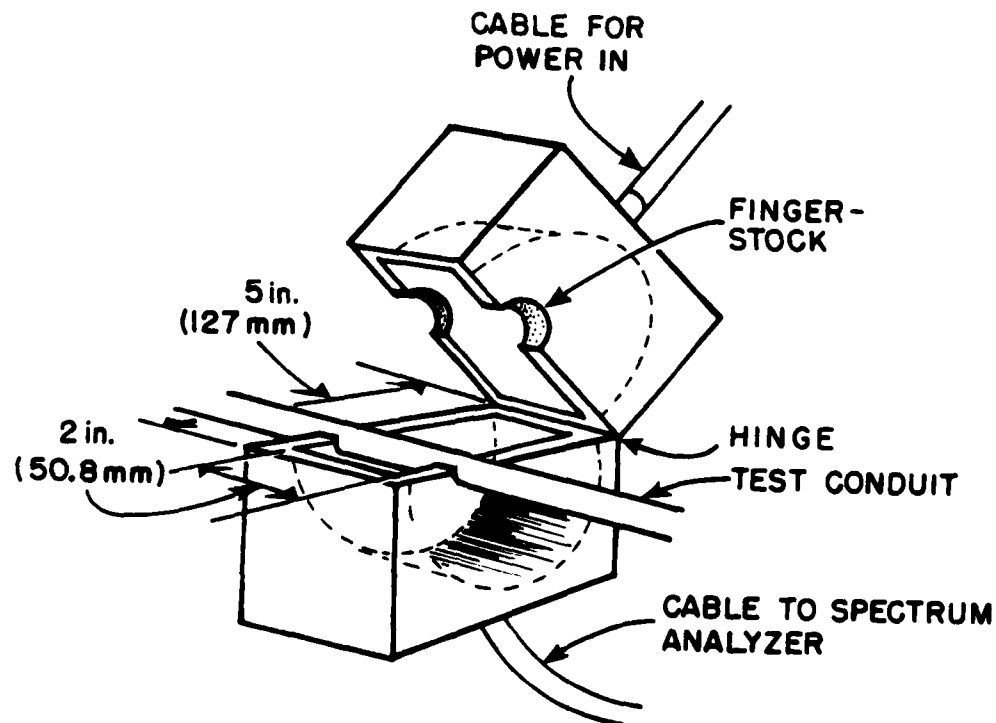


Figure 21. Resonant cavity for 1/2-in. (12.7-mm) EMT.

Five different conduit conditions were used for the evaluation:

<u>Condition</u>	<u>Reading on Receiver</u>
1. Solid conduit	5 to 8 V*
2. Transverse slot half-way through conduit	20 to 30 V
3. Transverse slot half-way through coupling	84 to 120 V
4. Longitudinal slot 1-in. (25.4-mm) long	20 V
5. Good coupling	10 to 25 V

The resonant frequency for each of these conditions was between 2.95 and 3.05 GHz.

The wire in the conduit was 12-gauge, solid copper terminated in 56 ohms at each end, this being the approximate characteristic impedance of a 12-gauge wire in a 1/2-in. (12.7-mm) conduit. The noise level of the receiver with a zero signal reading was 5 V. The data show the maximum range of values obtained for each condition. The readings were sensitive to the position of the test leads. This can be expected at the frequencies tested since the coaxial system formed by the wire and conduit is quite lossy, and the inductive loop formed by the resistive termination inside the shielded room is an unpredictable impedance at this frequency.

It is apparent that this test can identify the defects examined in the evaluation and may be useful for determining the EMP hardness of conduit systems. The disadvantages of this concept include (1) a requirement for access to the conduit; (2) a separate test fixture for each size conduit; and (3) signal losses along the conduit-wire coaxial system which may limit the concepts application for long systems.

The power available for this test was 1 mW. The cavity could absorb significantly higher power, probably 10 W or more, thus increasing detected signal levels by 40 dB, which means that relatively minor defects could be detected by this technique.

#### Standing Wave Defect Location Concept

If a transmission line terminating in a short circuit is excited with an ac signal, standing waves will be present on the transmission line. This means that voltage peaks and nodes exist along the length of the line. The peaks and nodes will occur at different locations on the transmission line with different excitation frequencies; these locations can be accurately determined theoretically. This suggests a possible test for locating conduit defects: a transmission line can be made up of a pair of conduits terminated

\* The receiver noise level was approximately 5 to 6 V.

with a short circuit on a shielded room. A conductor inside the conduit with a defect will be excited by the standing wave. By monitoring the signal level on the conductor as the applied frequency is varied, it should be possible to determine the location of a defect in the conduit. A schematic drawing of a test configuration to study the feasibility of this concept is shown in Figure 22. The conduit transmission line is excited with the variable frequency generator and RF power amplifier. The standing waves can be detected by observing the magnitude of the output of a current probe placed on one of the conduits. Figure 23 shows the current standing wave configuration for a parallel conduit system of 20 ft (6.1 m) of 1/2-in. (12.7-mm) steel EMT spaced 2-in. (50.8-mm) apart for frequencies from 4 MHz to 68 MHz.

Defects can be located by exciting the conduit transmission line at various frequencies, keeping constant the magnitude of the maximum conduit

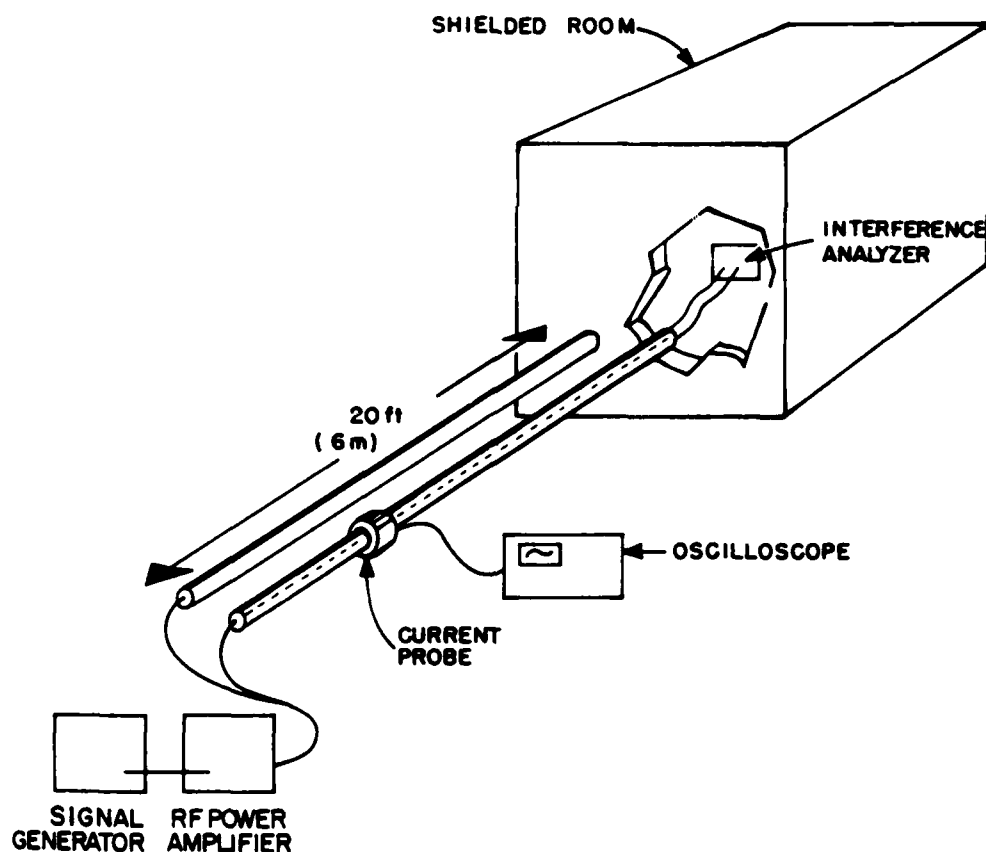


Figure 22. Conduit defect location by standing waves.

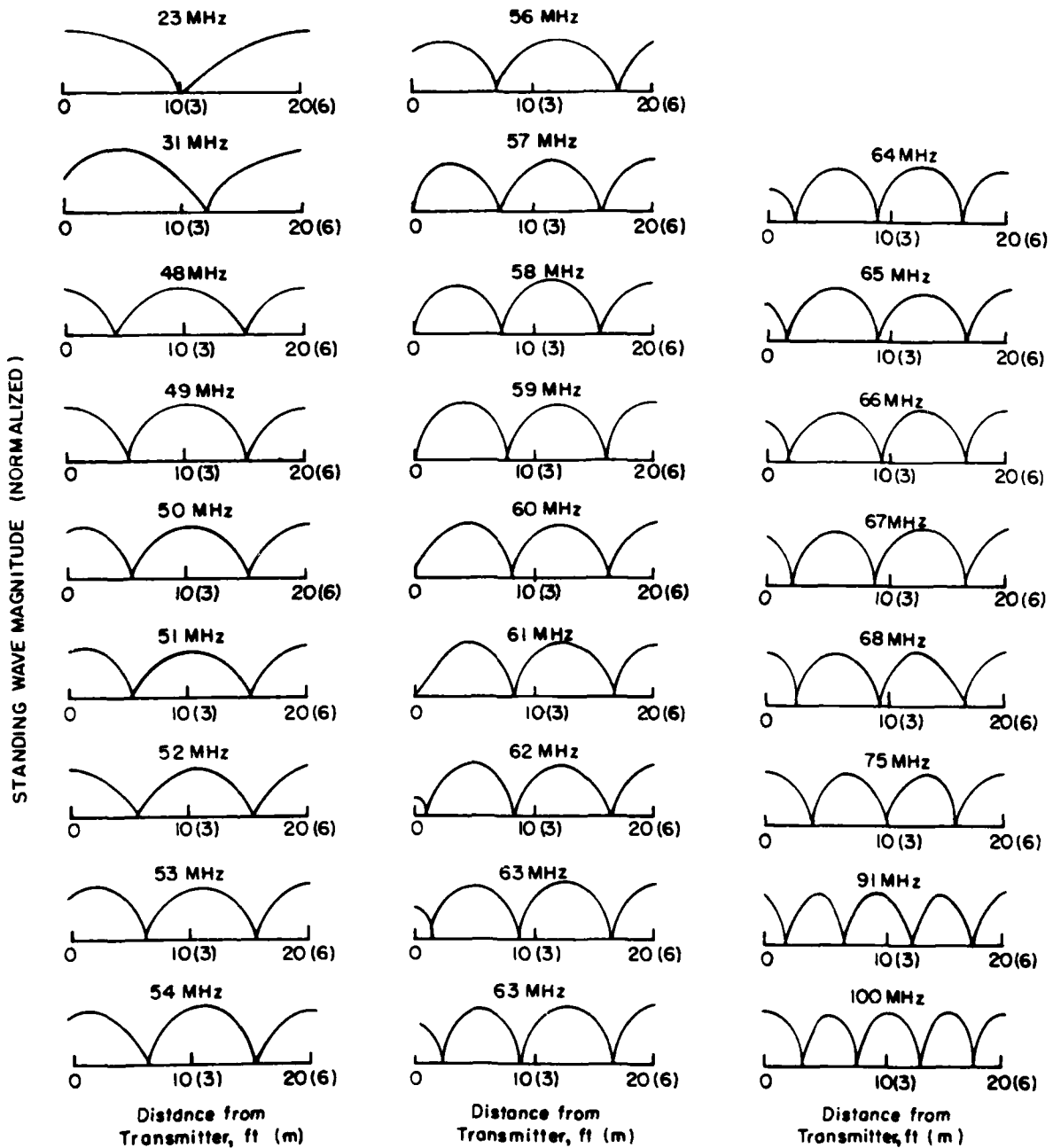


Figure 23. Standing waves on a shorted, two-conduit transmission line.

current, and monitoring the signal level appearing on the wire within the conduit. The magnitude of the detected signal is recorded and can be plotted. Peaks and minimums should appear when peaks and minimums from the standing wave coincide with the conduit defect. This experiment was done with the 20-ft (6.1-m) conduit system described for the previous test. Two tests were conducted: one with a slot cut half-way through a coupling (a defect at 10 ft [3 m] from the signal source) and one with a slot cut half-way through the conduit 4 ft (1.2 m) from the signal source, but with a good coupling installed. The following equipment was used: an HP 8601 signal generator, an ENI Model 310L RF power amplifier, a Stoddard 91550 current probe, a Tektronix 454 oscilloscope, and an EMC 25 MKIII interference analyzer. The current probe was placed on the conduit at the end where it was connected to the shielded room. Its output was monitored on the oscilloscope and kept constant as the frequency was varied. Since the end was shorted, a current maximum would always occur at this point. The data from these tests are plotted in Figures 24 and 25.

Comparison of the plots in Figures 24 and 25 with the standing wave data in Figure 23 shows that the concept works and a defect can be located. The results plotted in Figure 25 are interesting. The defect was located 4 ft (1.2 m) from one end of the conduit; a good EMT coupling joined the conduit with the defect to another 10-ft (3-m) conduit. The data show a small irregularity at the 10-ft (3-m) location. EMT couplings generally do not provide satisfactory EMP hardening, and in this case, the coupling shows up as a minor defect at 10 ft (3 m). Thus, the technique can be used to locate multiple defects. For a field-test system, the location of the standing-wave peaks and minimums can be theoretically determined -- they are spaced at half the free-space wavelength.

Although no tests were conducted to compare defect severity found by this technique with EMP leakage, the technique appears to be relatively sensitive and will locate all types of flaws causing EMP leakage.

The standing wave test would probably not be feasible for buried conduit since any transmission line in a conducting medium (soil) will be quite lossy.

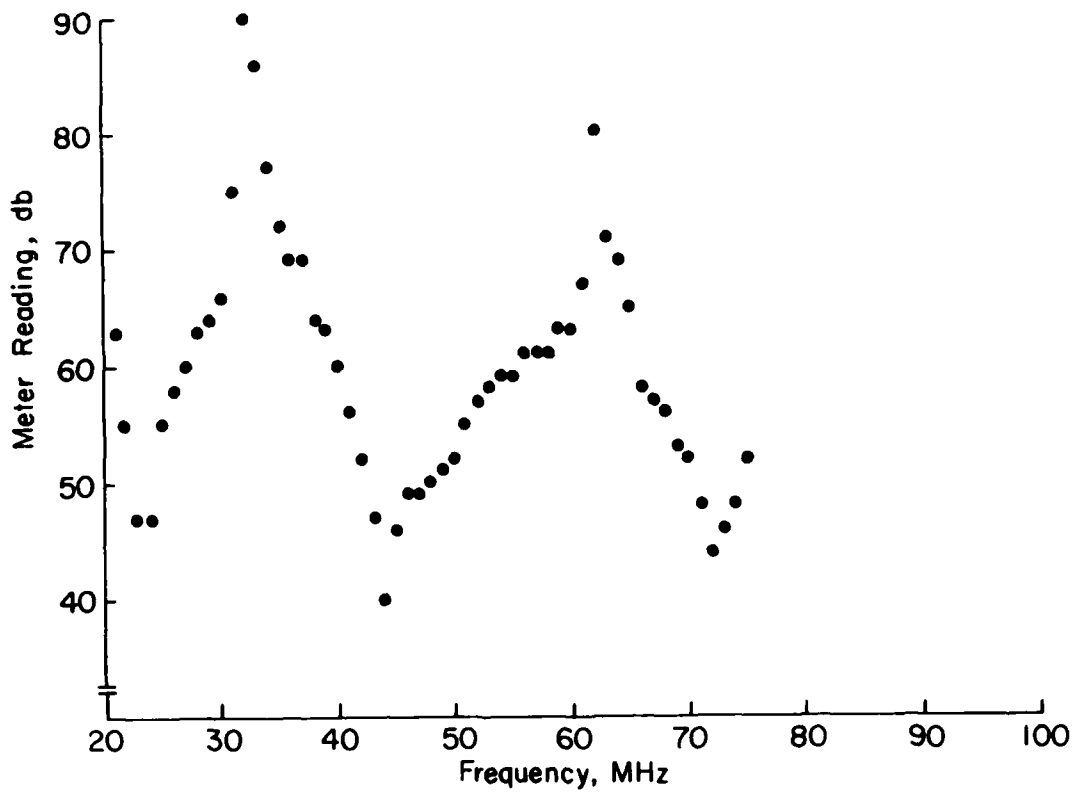


Figure 24. Standing wave defect location concept feasibility test-signal with a defect 10 ft (3 m) from end.

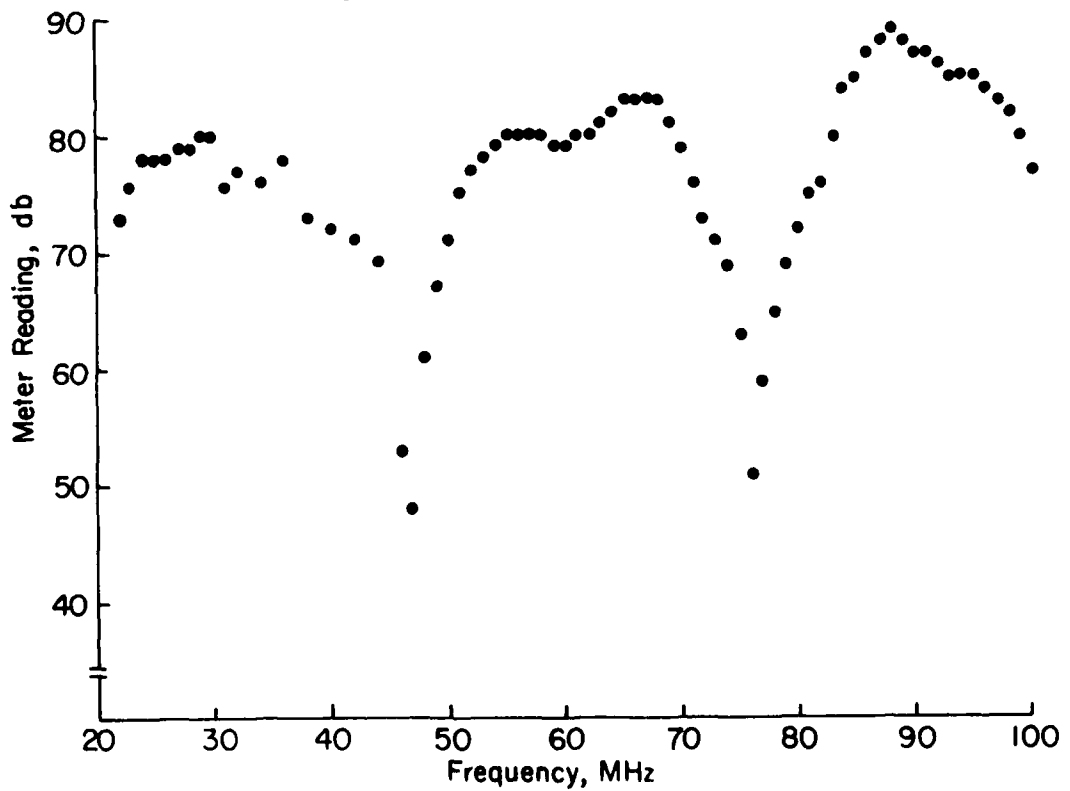


Figure 25. Standing wave defect location concept feasibility test-signal with defect 4 ft (1.2 m) from end.

## 5 DIFFUSION CURRENT ANALYSIS

EMP current flowing on the outside of a conduit will propagate through the conduit wall, creating a voltage drop on the inside surface. This voltage drop can, in turn, induce a current on conductors inside the conduit. Because of the skin effect phenomena, the high-frequency content of the driving pulse is attenuated much more than the low-frequency content, and the pulse appearing on the inside of the conduit is slower than the driving pulse. The actual wave shape of the diffusion pulse is a function of the conduit's thickness and material properties (electrical conductivity and magnetic permeability).

The method described here to determine the characteristics of the diffusion signal is based on an impulse response analysis which uses a planar approximation of the conduit's cylindrical geometry. This analysis requires that the system's response be slow in comparison to the applied pulse. This is true for most EMP wave shapes and conduit materials. The method can also be used for higher resistivity materials such as lead and stainless steel. For some of these materials, the penetration time may be on the same order of magnitude as the typical EMP duration; the accuracy to which the method can be used to calculate the diffusion pulse for these materials is considerably reduced. The analysis assumes a single conductor in the conduit. While this will rarely be the case except for coaxial cables (to which the analysis can also be applied), it is a reasonable approach since -- if there is more than one conductor -- the diffusion current signal will tend to divide among the conductors relative to termination resistance and wire size. The largest current will appear in the conductor with the smallest terminating resistance or the one with the largest cross-sectional area if terminating resistances are equal. Thus, the single conductor calculation is a worst-case analysis. (Sample problems using this analysis and the leakage current analysis are given in the Appendix.) A general solution (assuming constant permeability and conductivity) can be determined by calculating the time response of the conduit due to an impulse of electromagnetic energy, and then convoluting this response with any given pulse on the conduit. Similarly, the Fourier transform of the internal electric field resulting from an impulse current (referred to as the surface transfer impedance) can be multiplied by the Fourier transform of the current pulse to obtain the frequency domain solution for the electric field. (The detailed mathematical derivation for this technique is given in Appendix C of CERL Interim Report M-234).<sup>11</sup>

To simplify calculation of the electric field inside the conduit, the modified Bessel functions appearing in the Laplace transform of the electric field are replaced in this model by their asymptotic expansions. The results obtained using the asymptotic form of the Bessel functions are valid for cylindrical shields that have inner radii which are large compared to the skin depth of the lowest frequency of interest in the surface current pulse.\* Two

<sup>11</sup>W. Croisant, P. Nielsen, D. Sieber, and R. G. McCormack, Development of a Conduit Design Analytical Procedure, Interim Report M-234/ADAO56218 (CERL, June 1978).

\* It is shown in Appendix C of CERL Interim Report M-234 that the  $a$  (radius) to  $\delta$  (skin depth) ratio is 10 for a 1-in. (25.4-mm) steel conduit at a frequency of 200 kHz, assuming values of 150 for the relative permeability and  $20 \times 10^{-8}$  ohm-m for the resistivity.

infinite series solutions for the electric field due to current impulse have been developed -- one which converges for early times (Eq 1) and one which converges for late time (Eq 2):

$$E(a, \theta) = Q \left[ \frac{8}{\pi^{3/2} ab \mu \sigma^2 (b-a)^3} \right] \quad [\text{Eq 1}]$$

$$\left\{ \sum_{n=0}^{\infty} \frac{\exp - \left[ \frac{(2n+1)^2}{\theta} \right]}{\theta^{3/2}} \left[ \frac{(2n+1)^2}{\theta} - 1/2 \right] \right\}$$

$$\theta \geq \theta$$

$$E(a, \theta) = Q \left[ \frac{8}{\pi^{3/2} \sqrt{ab} \mu \sigma^2 (b-a)^3} \right] \left\{ \frac{\sqrt{\pi}}{2} \left[ \sum_{n=0}^{\infty} (-1)^{n+1} \frac{n^2 \pi^2}{4} \right] \exp \left( -\frac{n^2 \pi^2}{4} \theta \right) \right\}, \theta > \theta \quad [\text{Eq 2}]$$

where E = internal electric field

Q = injected charge

a = inner radius

b = outer radius

$\sigma$  = conductivity

$\mu$  = permeability

$\theta$  = relative time expressed in units of a characteristic diffusion time  $\theta = t/T$

$$T = \frac{\mu \sigma (b-a)^2}{4}$$

E(a,  $\theta$ ) can be put in the form:

$$E(a, \theta) = QFS(\theta) \quad [\text{Eq 3}]$$

where Q = charge passed along the cylinder

$$F = \frac{8}{\pi^{3/2} \sqrt{ab} \mu \sigma^2 (b-a)^3}$$

$$\theta = t/T$$

S( $\theta$ ) = the two series representations denoted by braces in Eqs 1 and 2.

Thus, the unit impulse response for a circular cylinder of a specified size and material can be defined by the shield parameters T and F, which depend on the dimensions and material properties of the cylinder. Investigation showed that these two parameters can be easily determined experimentally,

which is important since the material properties of conduits are not readily known.<sup>12</sup> Experimentation also indicated that once the parameters for one size cylinder (or conduit) of a given material are known, the parameters for another size cylinder of the same material can be found.

The electric field for a current pulse ( $I_C$ ), other than an impulse, can be determined by convolution with the impulse response (Eq 1 and Eq 2):

$$E(a, t) = QF \int_0^t I_C(t-\lambda) S(\lambda/T) d\lambda \quad [\text{Eq 4}]$$

where E = internal electric field  
 Q = injected charge  
 F =  $\frac{1}{8}$   
 $I_C$  =  $\frac{\pi^{3/2} \sqrt{ab} \mu\sigma^2 (b-a)^3}{4}$  current pulse  
 S = series representations of impulse response  
 t = time  
 T = diffusion time  $\frac{\mu\sigma(b-a)^2}{4}$   
 $\lambda$  = an integration variable.

Appendix C of CERL Report M-234 provides the detailed theoretical analysis and experimental evaluation of this model. The model assumes linearity; however, some deviations may occur at high current levels (saturation effects). Several examples of the impulse response, as well as results for other currents, were presented and compared with the experimental results and were found to be in excellent agreement. To apply this method to EMP hardened conduit system design, the following steps are necessary:

1. Determine the physical properties (conductivity, permeability, and dimensions) of the proposed conduit system. Typical resistivities and conductivities for conduit materials are given in Table 6. Most commercial electrical conduits are either aluminum or low-carbon steel. The relative permeability for most materials is 1; the exceptions are ferromagnetic materials such as iron and steel. The values of permeability for most conduit-grade steels fall in the range of 50 to 200. Most stainless steels are nonmagnetic, but some exhibit ferromagnetic behavior. Properties of conduit-grade materials are not well documented; however, a value of 130 for the relative permeability of steel conduit has been experimentally determined.<sup>13</sup> In the absence of more accurate information for a specific sample, this value seems reasonable to use for the calculations described here.

The dimensions of interest for commercial conduits are given in Tables 7 (for rigid conduit), 8 (for intermediate wall conduit), and 9 (for electrical metallic tubing or thin-walled conduit).

<sup>12</sup>W. Croisant, P. Nielsen, D. Seiber, and R. G. McCormack, Development of a Conduit Design Analytical Procedure, Interim Report M-234/ADA056218 (CERL, June 1978), Appendix C.

<sup>13</sup>Croisant et al.

Table 6  
Resistivity and Conductivity for Materials  
Used for Electrical Conduits\*

	Resistivity (Ohm-CentiMeter x 10 <sup>-6</sup> )	Conductivity (Mhos per Meter)
Aluminum	2.62	3.82 x 10 <sup>7</sup>
Brass	3.9	2.56 x 10 <sup>7</sup>
Copper	1.7241	5.80 x 10 <sup>7</sup>
Iron	9.71	1.03 x 10 <sup>7</sup>
Lead	98	1.02 x 10 <sup>6</sup>
Steel (0.4-0.5% Carbon)	13-22	4.55-7.69 x 10 <sup>6</sup>
Steel (Manganese)	70	1.43 x 10 <sup>6</sup>
Steel (Stainless)	90	1.11 x 10 <sup>6</sup>
Tin	11.4	8.77 x 10 <sup>6</sup>
Zinc	35.3	2.83 x 10 <sup>6</sup>

\*For additional information, see, for example, Electronics Engineer's Handbook (McGraw-Hill Book Company, 1975), p 6-4, or Reference Data for Radio Engineers, Sixth Edition (Howard W. Sams & Co., Inc., pp 4-21 to 4-22.

Table 7  
Nominal Dimensions and Parameters of  
Ferrous Metal and Aluminum Rigid Conduit

Nominal Size of Conduits, In. (mm)	Inner Diameter, In. (mm)	Outer Diameter, In. (mm)	Wall Thickness, In. (mm)
1/4 (6)	0.364 (9.246)	0.540 (13.72)	0.088 (2.235)
3/8 (10)	0.493 (12.52)	0.675 (17.15)	0.091 (2.311)
1/2 (13)	0.622 (15.80)	0.840 (21.34)	0.109 (2.769)
3/4 (19)	0.824 (20.93)	1.050 (26.67)	0.113 (2.870)
1 (25)	1.049 (26.64)	1.315 (33.40)	0.133 (3.378)
1-1/4 (32)	1.380 (35.05)	1.660 (42.16)	0.140 (3.556)
1-1/2 (38)	1.610 (40.89)	1.900 (48.26)	0.145 (3.683)
2 (51)	2.067 (52.50)	2.375 (60.33)	0.154 (3.912)
2-1/2 (63)	2.469 (62.71)	2.875 (73.03)	0.203 (5.156)
3 (76)	3.068 (77.93)	3.500 (88.90)	0.216 (5.486)
3-1/2 (89)	3.548 (90.12)	4.000 (101.6)	0.226 (5.740)
4 (102)	4.026 (102.3)	4.500 (114.3)	0.237 (6.020)
5 (127)	5.047 (128.2)	5.563 (141.3)	0.258 (6.553)
6 (152)	6.065 (154.1)	6.625 (168.3)	0.280 (7.112)

2. Estimate the charge transported by the conduit current. The method of analyzing diffusion current assumes an impulse driving function -- i.e., an applied pulse short in duration relative to the conduit's response time. The important variable in this analysis is the total charge transported by the conduit current. This can generally be found by integrating the current waveform.

3. Calculate diffusion time constant. The diffusion time constant (a variable necessary for later calculations) is determined by the following formula:

$$T = \frac{\mu\sigma (b-a)^2}{4} \text{ microseconds} \quad [\text{Eq 5}]$$

where  $\mu$  = permeability (henries per meter)  
 $\sigma$  = conductivity (mhos per meter)  
 $b-a$  = the thickness of the conduit (meters).

The time the peak amplitude or open circuit voltage occurs is  $0.367T$ , where  $T$  is the diffusion time constant. This value (0.367) results from use of the series representation  $S(\theta)$  for the shape of the diffusion pulse.

4. Determine the peak value of open-circuit voltage. The peak amplitude of the voltage induced on a conductor inside a conduit by diffusion if the conductor is terminated in an open circuit (effectively 100 ohms or greater) can be found by:

$$V_{oc} = 0.656 QF\ell \quad [\text{Eq 6}]$$

where  $Q$  equals the injected charge in coulombs, and  $\ell$  = the conduit length of interest in meters, and:

$$F = \frac{8}{\pi^{3/2} \sqrt{ab} \mu\sigma^2 (b-a)^3} \quad [\text{Eq 7}]$$

where  $a$  = the inner radius of the conduit in meters  
 $b$  = the outer radius in meters  
 $\mu$  =  $4\pi \times 10^{-7} \times \mu_r$  in henries per meter.

(The value, 0.656, also results from the series representation,  $S(\theta)$ , for the diffusion pulse.)

Table 8  
Intermediate Metal Conduit (IMC) Dimensions\*

Trade Size, In. (mm)	IMC Type I		IMC Type II		IMC Type II			
	Diameter, In. (mm)		Wall Thickness, In. (mm)**		Outside Diameter, In. (mm)		Wall Thickness, In. (mm)+	Length of Finished IMC, Ft. In. (m)
	Minimum	Maximum	Minimum	Maximum	Minimum	Maximum		
1/2 (13)	0.810 (20.57)	0.820 (20.83)	0.070 (1.778)	0.825 (20.96)	0.840 (21.34)	0.00 (2.032)	9 11-1/4 (3.03)	
3/4 (19)	1.024 (26.01)	1.034 (26.26)	0.075 (1.905)	1.035 (26.29)	1.050 (26.67)	0.085 (2.159)	9 11-1/4 (3.03)	
1 (25)	1.285 (32.64)	1.295 (32.89)	0.085 (2.159)	1.300 (33.02)	1.315 (33.40)	0.105 (2.667)	9 11 (3.02)	
1-1/4 (32)	1.630 (41.40)	1.645 (41.78)	0.085 (2.159)	1.645 (41.78)	1.660 (42.16)	0.108 (2.743)	9 11 (3.02)	
1-1/2 (38)	1.875 (47.63)	1.890 (48.01)	0.090 (2.032)	1.885 (47.88)	1.900 (48.26)	0.108 (2.743)	9 11 (3.02)	
2 (51)	2.352 (59.74)	2.367 (60.12)	0.095 (2.413)	2.360 (59.94)	2.375 (60.33)	0.108 (2.743)	9 11 (3.02)	
2-1/2 (64)	2.847 (72.31)	2.867 (72.82)	0.130 (3.302)	2.850 (72.39)	2.875 (73.03)	0.155 (3.937)	9 10-1/2 (3.01)	
3 (76)	3.466 (88.04)	3.486 (88.54)	0.130 (3.302)	3.475 (88.27)	3.500 (88.90)	0.155 (3.937)	9 10-1/2 (3.01)	
3-1/2 (89)	3.961 (100.61)	3.981 (101.1)	0.130 (3.302)	3.975 (101.0)	4.000 (101.6)	0.160 (4.064)	9 10-1/4 (3.00)	
4 (102)	4.456 (113.2)	4.476 (113.7)	0.130 (3.302)	4.475 (113.7)	4.500 (114.3)	0.160 (4.064)	9 10-1/4 (3.00)	

\*From UL, Inc., Revision of the Outline of the Proposed Investigation for Intermediate Metal Conduit (May 24, 1977), Table 8.1. The complete publication is available from Publication Stock of UL at 333 Pfingsten Road, Northbrook, IL 60062.

\*\*Tolerance +0.015 in. (0.381 mm) for 1/2 through 2 in. (13 through 51 mm)

Type I: +0.020 in. (0.508 mm) for 2-1/2 through 4 in. (64 through 102 mm)  
-0.000 in. (0.000 mm) for 1/2 through 4 in. (13 through 102 mm)

\*Tolerance +0.020 in. (0.508 mm) for 1/2 through 2 in. (13 through 51 mm)

Type II: +0.025 in. (0.685 mm) for 2-1/2 through 4 in. (64 through 102 mm)  
-0.000 in. (0.000 mm) for 1/2 through 4 in. (64 through 102 mm)

Table 9

## Dimensions of Electrical Metallic Tubing (Thin-Walled Conduit)\*

Trade Size of Tubing, In. (mm)	External Diameter, In. (mm)	Internal Diameter, In. (mm)	Wall Thickness, In. (mm)
3/8 (10)	0.577 + 0.005 (14.66 + 0.127)	0.493 (12.52)	0.042 (1.067)
1/2 (13)	0.706 + 0.005 (17.93 + 0.127)	0.622 (15.80)	0.042 (1.067)
3/4 (19)	0.922 + 0.005 (23.42 + 0.127)	0.824 (20.93)	0.049 (1.245)
1 (25)	1.163 + 0.005 (29.54 + 0.127)	1.049 (26.64)	0.057 (1.448)
1-1/4 (32)	1.510 + 0.005 (38.35 + 0.127)	1.380 (35.05)	0.065 (1.651)
1-1/2 (38)	1.740 + 0.005 (44.20 + 0.127)	1.610 (40.89)	0.065 (1.651)
2 (51)	2.197 + 0.005 (55.80 + 0.127)	2.067 (52.50)	0.065 (1.651)
2-1/2 (64)	2.875 + 0.010 (73.03 + 0.254)	2.731 (69.37)	0.072 (1.829)
3 (76)	3.500 + 0.015 (88.90 + 0.381)	3.356 (85.24)	0.072 (1.829)
3-1/2 (89)	4.000 + 0.020 (101.6 + 0.711)	3.834 (97.38)	0.083 (2.108)
4 (102)	4.500 + 0.020 (114.3 + 0.711)	4.334 (110.1)	0.083 (2.108)

\*From UL Inc., Standard for Electrical Metallic Tubing, Fourth Edition, Standard 797 (August 19, 1977), Table 4.2. The complete publication is available from Publication Stock of UL at 333 Pfingsten Road, Northbrook, IL 60062.

\*\*Not a requirement; included for information only.

5. Determine conduit-wire circuit parameters (resistance and inductance). The resistance of the wire is:

$$R_{\text{wire}} = \frac{\ell \rho}{A} = \frac{\ell}{A \sigma} \quad [\text{Eq 8}]$$

where  $\ell$  = length  
 $\rho$  = resistivity  
 $A$  = cross-sectional area  
 $\sigma$  = conductivity.

Similarly, the resistance of the conduit is:

$$R_{\text{conduit}} = \frac{\ell}{A \sigma} \quad [\text{Eq 9}]$$

where the cross-sectional area of the conduit is  $A$  equals  $(b^2 - a^2)$ ,  $b$  equals outer diameter, and  $a$  equals inner diameter.

Table 10 gives the resistances in ohms per meter for wire sizes likely to be used in conduits; Table 11 gives the resistance per meter of standard steel conduits at conductivities of  $4.55 \times 10^6$  and  $7.69 \times 10^6$  mho/m. (This is a range of conductivities for pipe steels, but conduits are generally made from the same materials and can be expected to have similar conductivities.)

Table 10  
Resistance of Annealed Copper Wire\*

Wire Gage	Ohms per Foot	Ohms per Meter
0000	$4.9 \times 10^{-5}$	$1.6 \times 10^{-4}$
000	$6.2 \times 10^{-5}$	$2.0 \times 10^{-4}$
00	$7.8 \times 10^{-5}$	$2.6 \times 10^{-4}$
0	$9.8 \times 10^{-5}$	$3.2 \times 10^{-4}$
1	$1.23 \times 10^{-4}$	$4.04 \times 10^{-4}$
2	$1.56 \times 10^{-4}$	$5.12 \times 10^{-4}$
3	$1.97 \times 10^{-4}$	$6.46 \times 10^{-4}$
4	$2.48 \times 10^{-4}$	$8.14 \times 10^{-4}$
5	$3.13 \times 10^{-4}$	$1.03 \times 10^{-3}$
6	$3.95 \times 10^{-4}$	$1.30 \times 10^{-3}$
7	$4.98 \times 10^{-4}$	$1.63 \times 10^{-3}$
8	$62.8 \times 10^{-4}$	$2.06 \times 10^{-3}$
9	$7.92 \times 10^{-4}$	$2.60 \times 10^{-3}$
10	$9.99 \times 10^{-4}$	$3.28 \times 10^{-3}$
12	$1.59 \times 10^{-3}$	$5.22 \times 10^{-3}$
14	$2.25 \times 10^{-3}$	$8.27 \times 10^{-3}$
16	$4.02 \times 10^{-3}$	$1.32 \times 10^{-2}$
18	$6.38 \times 10^{-3}$	$2.09 \times 10^{-2}$
20	$1.02 \times 10^{-2}$	$3.35 \times 10^{-2}$
22	$1.61 \times 10^{-2}$	$5.28 \times 10^{-2}$
24	$2.57 \times 10^{-2}$	$8.43 \times 10^{-2}$
26	$4.08 \times 10^{-2}$	$1.34 \times 10^{-1}$
30	$1.03 \times 10^{-1}$	$3.38 \times 10^{-1}$
40	1.05	3.44

\*For additional information, see, for example, Electronics Engineers' Handbook (McGraw-Hill Book Company, 1975), p 6-22, or Reference Data for Radio Engineers, Sixth Edition (Howard W. Sams & Co., Inc., 1975), p 4-50.

The inductance per unit length can be found by referring to Figure 26. The high-frequency inductance (L) is given by:

$$L = 2 \times 10^{-7} \ln \frac{R_2}{R_1} \text{ henries/m} \quad [\text{Eq 10}]$$

where  $R_1$  = radius of the conductor  
 $R_2$  = inner radius of the conduit.

Table 11  
Resistance of Rigid Steel Conduit  
(Ohms per Meter of Length)

Conduit Size, In. (mm)	Inner Diameter, In. (mm)	Outer Diameter, In. (mm)	R High, = $4.55 \times 10^6*$	R Low, = $9.69 \times 10^6*$
1/4 (6)	0.364 (9.246)	0.540 (13.72)	$2.722 \times 10^{-3}$	$1.610 \times 10^{-3}$
3/8 (10)	0.493 (12.52)	0.675 (17.15)	$2.030 \times 10^{-3}$	$1.201 \times 10^{-3}$
1/2 (13)	0.622 (15.80)	0.840 (21.34)	$1.343 \times 10^{-3}$	$7.948 \times 10^{-4}$
3/4 (19)	0.824 (20.93)	1.050 (26.67)	$1.050 \times 10^{-3}$	$6.211 \times 10^{-4}$
1 (25)	1.049 (26.64)	1.315 (33.40)	$6.859 \times 10^{-4}$	$4.058 \times 10^{-4}$
1-1/4 (32)	1.380 (35.05)	1.660 (42.16)	$5.034 \times 10^{-4}$	$2.979 \times 10^{-4}$
1-1/2 (38)	1.610 (40.89)	1.900 (48.26)	$4.357 \times 10^{-4}$	$2.578 \times 10^{-4}$
2 (51)	2.067 (52.50)	2.375 (60.33)	$3.101 \times 10^{-4}$	$1.835 \times 10^{-4}$
2-1/2 (63)	2.469 (62.71)	2.875 (73.03)	$1.972 \times 10^{-4}$	$1.167 \times 10^{-4}$
3 (76)	3.068 (77.93)	3.500 (88.90)	$1.347 \times 10^{-4}$	$7.969 \times 10^{-5}$
3-1/2 (89)	3.548 (90.12)	4.000 (101.6)	$1.271 \times 10^{-4}$	$7.523 \times 10^{-5}$
4 (102)	4.026 (102.3)	4.500 (114.3)	$1.073 \times 10^{-4}$	$6.350 \times 10^{-5}$
5 (127)	5.047 (128.2)	5.563 (141.3)	$7.925 \times 10^{-5}$	$4.689 \times 10^{-5}$
6 (152)	6.065 (154.1)	6.625 (168.3)	$6.106 \times 10^{-5}$	$3.613 \times 10^{-5}$

\*To find resistance in ohms per foot, divide table values by 3.28.

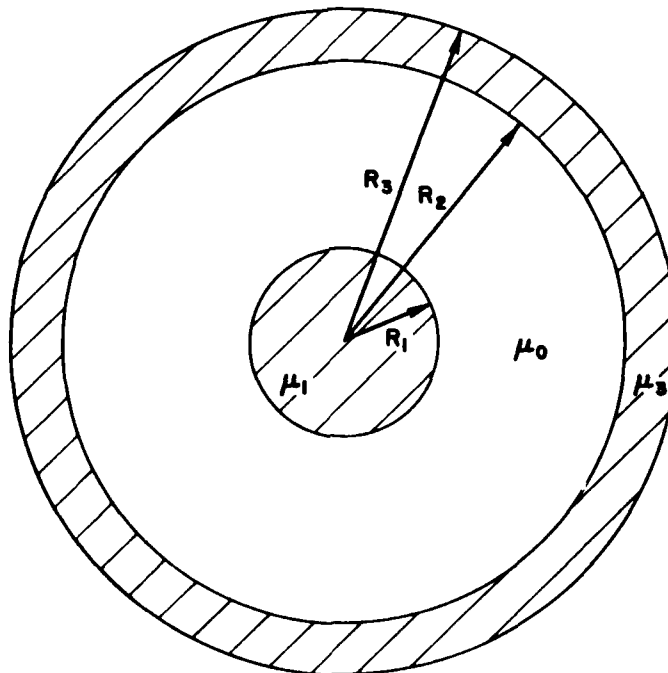


Figure 26. Coaxial conduit-wire system.

This equation assumes a central location for the conductor; an experimental verification was done without centering the conductor, but the results were reasonably close to the theoretically determined values.<sup>14</sup> The inductance for each conductor will be essentially identical for multi-conductors in the conduit if the conductors are the same size.

An added refinement which will not be necessary for most applications, but which allows an accurate representation of the decreasing portion of the diffusion pulse, is the low-frequency inductance:

$$L = 2 \times 10^{-7} \left[ \frac{\mu_1}{4\mu_0} + \ln \frac{R_2}{R_1} + \frac{\mu_3}{\mu_0} \left( \frac{R_3^4}{(R_3^2 - R_2^2)^2} \ln \frac{R_3}{R_2} - \frac{3R_3^2 - R_2^2}{4(R_3^2 - R_2^2)} \right) \right] \text{ [Eq 11]}$$

where  $R_3$  = outer radius of the conduit

$\mu_1$  = permeability of the inner conductor

$\mu_0$  = permeability of the space between the inner conductor and the conduit

$\mu_3$  = permeability of the conduit.

The high-frequency inductance applies to frequencies where most of the current is concentrated on the outer surface of the conduit; the low-frequency inductance takes into account the effects of the material properties of the wire and conduit.

Values of high-frequency inductance for commercial conduit and different conductor sizes are given in Table 12.

6. Determine short-circuit current amplitude. The peak value of the short-circuit current can be found from:

$$\begin{aligned} I_{sc} &= \frac{V_{oc} \sqrt{\pi}}{0.656 \times 2L} \times (\text{Peak Amplitude Factor}) & \text{ [Eq 12]} \\ &= \frac{1.351T V_{oc}}{L} (\text{Peak Amplitude Factor}) \end{aligned}$$

where  $V_{oc}$  is the previously determined value for the open-circuit voltage.

<sup>14</sup>W. Croisant, P. Nielsen, D. Sieber, and R. G. McCormack, Development of a Conduit Design Analytical Procedure, Interim Report M-234/ADA056218 (CERL, June 1978), Appendix C.

Table 12

High Frequency Inductance of Wire-Conduit System (in Microhenries per Meter)\*  
Wire Gauge

Conduit Size, In. (mm)	Wire Gauges										
	0000	000	00	0	1	2	3	4	5	8	9
1/4(6)	1.41 x 10 <sup>-2</sup>	3.77 x 10 <sup>-2</sup>	6.05 x 10 <sup>-2</sup>	2.26 x 10 <sup>-2</sup>	4.58 x 10 <sup>-2</sup>	6.9 x 10 <sup>-2</sup>	9.22 x 10 <sup>-2</sup>	0.115	0.163	0.208	0.231
3/8(10)	6.04 x 10 <sup>-2</sup>	8.39 x 10 <sup>-2</sup>	0.107	8.37 x 10 <sup>-2</sup>	0.107	0.130	0.153	0.176	0.224	0.269	0.292
1/2(13)	0.117	0.141	0.164	0.130	0.153	0.176	0.199	0.223	0.270	0.315	0.339
3/4(19)	0.165	0.188	0.217	0.187	0.210	0.233	0.256	0.280	0.327	0.372	0.396
1-1/4(32)	0.219	0.243	0.266	0.234	0.257	0.280	0.304	0.327	0.374	0.420	0.443
1-1/2(38)	0.251	0.275	0.297	0.289	0.312	0.335	0.359	0.382	0.429	0.474	0.498
2(51)	0.300	0.324	0.346	0.321	0.344	0.367	0.390	0.413	0.461	0.506	0.530
2-1/2(63)	0.336	0.359	0.382	0.370	0.393	0.416	0.439	0.462	0.510	0.555	0.478
3(76)	0.379	0.403	0.426	0.405	0.428	0.452	0.475	0.498	0.546	0.591	0.614
3-1/2(84)	0.408	0.432	0.455	0.445	0.468	0.491	0.514	0.538	0.585	0.630	0.654
4(102)	0.434	0.457	0.480	0.478	0.501	0.524	0.548	0.571	0.618	0.664	0.687
5(127)	0.479	0.502	0.526	0.503	0.527	0.550	0.573	0.596	0.644	0.689	0.712
6(152)	0.516	0.539	0.562	0.549	0.572	0.595	0.618	0.641	0.689	0.734	0.757
1/4(6)	0.254	0.303	0.347	0.393	0.440	0.486	0.533	0.579	0.626	0.719	0.794
3/8(10)	0.316	0.364	0.408	0.455	0.501	0.547	0.594	0.640	0.687	0.780	1.01
1/2(13)	0.362	0.410	0.454	0.501	0.547	0.594	0.640	0.687	0.733	0.826	1.06
3/4(19)	0.419	0.467	0.511	0.558	0.604	0.651	0.697	0.744	0.790	0.883	1.11
1(25)	0.466	0.515	0.559	0.605	0.652	0.698	0.744	0.791	0.837	0.930	1.16
1-1/4(32)	0.521	0.569	0.614	0.660	0.705	0.753	0.799	0.846	0.892	0.985	1.22
1-1/2(38)	0.552	0.601	0.645	0.691	0.738	0.784	0.831	0.877	0.924	1.02	1.25
2(51)	0.602	0.650	0.694	0.741	0.787	0.833	0.880	0.926	0.973	1.06	1.30
2-1/2(63)	0.637	0.686	0.730	0.776	0.823	0.869	0.915	0.962	1.01	1.10	1.33
3(76)	0.677	0.725	0.769	0.816	0.862	0.909	0.955	1.00	1.05	1.14	1.37
3-1/2(89)	0.710	0.759	0.803	0.849	0.895	0.942	0.988	1.03	1.08	1.17	1.40
4(102)	0.735	0.784	0.828	0.875	0.921	0.967	1.01	1.06	1.11	1.20	1.43
5(127)	0.781	0.829	0.873	0.914	0.966	1.01	1.06	1.10	1.15	1.24	1.48
6(152)	0.817	0.866	0.910	0.956	1.00	1.05	1.09	1.14	1.19	1.28	1.51

\* To determine inductance in microhenries per foot, multiply by 3.28.

The peak amplitude factor is obtained from Figure 27 after  $\alpha$  is determined from the formula

$$\alpha = TR/L \quad [Eq 13]$$

where T = the diffusion time constant of the conduit  
 R = the total short circuit resistance of the wire-conduit system  
 L = the inductance of the system.

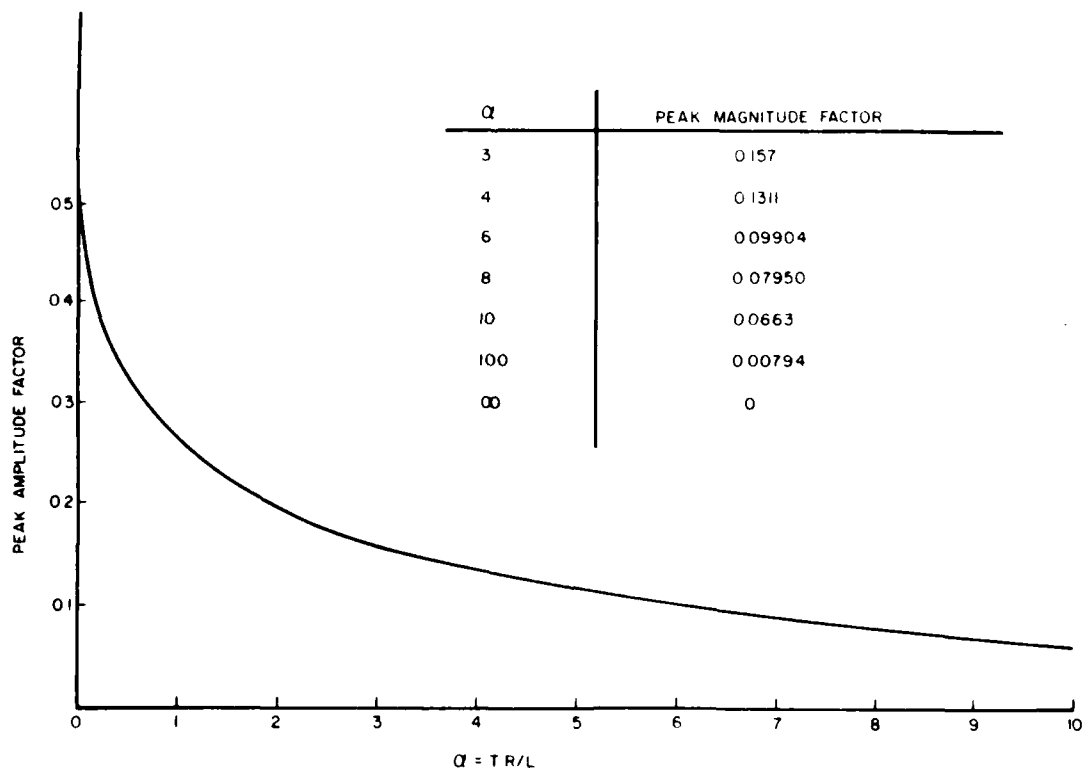


Figure 27. Peak amplitude factor versus.

## 6 DEFECT LEAKAGE MECHANISM

The basic shielding of a conduit system is provided by the solid conduit itself. However, defects in the conduit, such as cracks and breaks, may seriously compromise the shielding. In addition, because the many fittings and related hardware items (e.g., couplings, unions, case access fittings, pull boxes, junction boxes, flexible sections) used in conduit systems have not been designed to be EMP hardened, they may also compromise the shielding of the system. Thus, assessing the EMP penetration of the entire conduit system requires that the contribution of various defects, conduit fittings, and hardware items be evaluated.

Voltages resulting from hardware or defect leakage induced on conductors within conduit are likely to have complex waveforms which depend on a number of factors, including:

1. The waveform of the conduit current.
2. The nature and characteristics of the defect.
3. The proximity of internal conductors to the defect.
4. The type of internal conductor.
5. The transmission line characteristics of the coaxial system formed by the internal conductor and the conduit.
6. The termination of the internal conductor.

The peak voltage induced on internal conductors by leakage can be much greater than the peak voltage induced by diffusion through a jointless shield. However, the duration of the leakage-related transient is much shorter than the diffusion-related transient; thus, total energy content is likely to be less for the leakage current.

Leakage current analysis is complicated by the varied and often irregular geometrics associated with defects and fittings. Since an exact mathematical analysis of even relatively simple defects, conduit fittings, and hardware items is very difficult (and in some cases, nearly impossible), some reliance must necessarily be placed on empirical results. The analytical methods presented here are based on relatively simple mathematical models describing both the significant features of leakage and the parameters which need to be determined for each item under consideration.

As with the diffusion current, the total leakage current will tend to divide among a number of conductors. Thus, a single conductor analysis will again be a worst case. The impedance seen by the leakage voltage generator (especially for electrically long lines) will be the characteristic impedance of the conduit-conductor transmission line rather than the terminating resistance, as is the case for the diffusion current.

## EMP Leakage Mechanisms

Leakage into a conduit involves: (1) series impedances at joints and connections, which includes a voltage component caused by resistances between segments; and (2) electromagnetic field coupling through apertures, which includes a mutual-coupling component caused by the penetration of the magnetic field through openings in the conduit, and a capacitive-coupling component caused by the penetration of the electric field through openings in the conduit.

### *Series Impedance at Joints and Connections*

Imperfect metallic contact at connections and joints produces an increase in the electrical resistance at that point. The current flowing on the exterior of the conduit creates a voltage drop that is coupled into the coaxial line formed by the conduit and internal conductor. The equivalent voltage source is represented by:

$$V(t) = RI(t) \quad [\text{Eq 14}]$$

where  $R$  is the resistance and  $I(t)$  the conduit current. The voltage is proportional to the current pulse flowing on the exterior of the conduit. In the frequency domain:

$$v(\omega) = Ri(\omega) \quad [\text{Eq 15}]$$

where  $i(\omega)$  is the frequency domain representation of the current.

For a pure resistive flaw impedance,  $Z$  equals  $R$  and is independent of frequency.

Since  $R$  is usually comparatively small, the equivalent-voltage generator may be considered to have zero internal resistance relative to the coaxial line formed by the conduit and internal conductor.

Because arcing is possible, the resistance of a rusted connection or joint may be quite different for small and large conduit currents. When the arcing threshold is exceeded, the internal conductor current has been observed to decrease. Thus, arcing tends to reduce the apparent connection resistance. Although most rusted joints tend to arc if the current is large enough, experimental results indicate that it is not possible to predict a specific threshold current at which arcing will begin. In general, possible arcing effects will be disregarded in the analytic methods described here.

### *Electromagnetic Field Coupling Through Apertures*

In the absence of an aperture, the magnetic flux lines associated with a conduit current form concentric circles about the conduit. With an aperture, some of the circumferential magnetic field associated with the conduit current can penetrate the aperture and couple with the internal conductor. The penetration of the magnetic field through an aperture in the conduit is shown in Figure 28. A mutual inductance then exists between the conduit circuit and the inner conductor circuit.

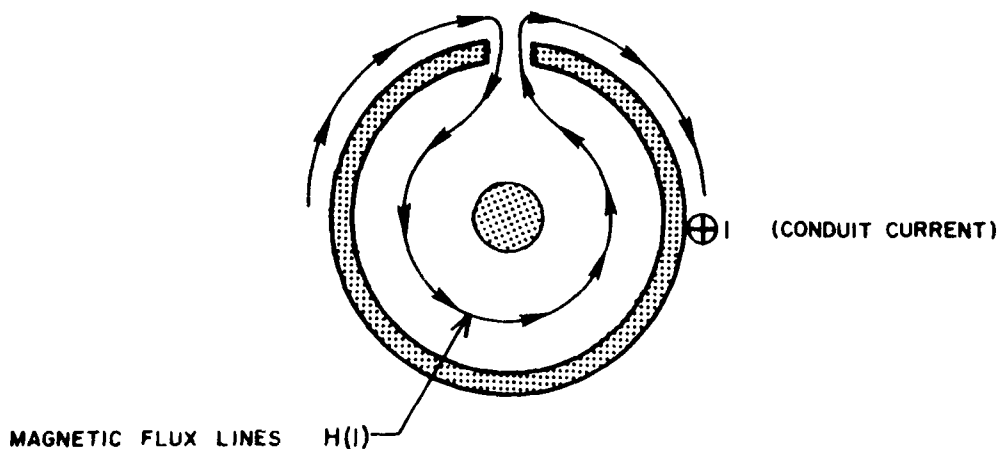


Figure 28. Magnetic field penetrating through an aperture in a conduit.

A zero impedance voltage source  $V$  for this aperture coupling can be represented by:

$$V(t) = M \frac{dI(t)}{dt} \quad [\text{Eq 16}]$$

where  $I(t)$  is the conduit current, and  $M$  is a mutual inductance coefficient which contains parameters associated with both the aperture and the coaxial line formed by the conduit and the inner conductor. Thus, it can be seen that the leakage through small apertures is proportional to the time derivative of the conduit current. For the purposes of this analysis,  $M$  will be known as the inductive coupling coefficient.

The Fourier transform of Eq 16 is:

$$v(\omega) = Mj\omega i(\omega) \quad [\text{Eq 17}]$$

where  $v(\omega)$  is the frequency-dependent voltage induced on the inner conductor, and  $i(\omega)$  is the conduit current. The inductive transfer impedance,  $Z = Mj\omega$ , increases linearly with frequency.

The value of the mutual coupling coefficient depends on the dimensions of the aperture, the orientation of the aperture with respect to the magnetic flux lines, and the position of the internal conductor relative to the aperture. A useful concept for theoretically determining the coupling coefficient is the magnetic polarizability, which will have a unique value for each type of aperture under consideration.\* Unfortunately, analytical expressions for

\* The magnetic polarizability for apertures in thin conducting sheets is the effective dipole strength on the "protected" side of the sheet produced by one unit (e.g., 1 A/m) of excitation field on the opposite side of the sheet. See A. L. Whitson and E. F. Vance, Bolt Lapped-Joint EMP Shield, DNA 4472-F (Defense Nuclear Agency, June 1977).

polarizabilities are not generally available for complicated apertures in cylinders; however, such values for a number of simple holes, including circles, ellipses, and thin slots in thin conducting sheets have been derived and expressed in terms of the dimensions of the aperture.<sup>15</sup> These quantities, shown in Table 13, can be used to estimate the approximate magnitude of M (the inductive coupling coefficient) for electrically small apertures in conduits, and to study the trends of this coupling coefficient as aperture parameters are varied.

For a concentric coaxial cylinder model, the mutual inductance or coupling coefficient (in henries) associated with an aperture is:

$$M = \frac{\mu_0 m}{4\pi a^2} \quad [\text{Eq 18}]$$

where  $m$  = the magnetic polarizability of the aperture  
 $\mu_0$  = the permeability of free space  
 $a$  = the radius of the conduit.

The effect of the size and orientation of the apertures is more apparent if a particular aperture is assumed, and the magnetic polarizability and mutual coupling coefficient are evaluated. For example, a small circular aperture of radius  $r$  has a polarizability of:

$$m = \frac{4}{3}r^3 \quad [\text{Eq 19}]$$

This gives a mutual coupling coefficient:

$$M = \frac{\mu_0 r^3}{3\pi a^2} \quad [\text{Eq 20}]$$

The inductive coefficient (and hence the induced voltage) is proportional to the cube of the radius; e.g., an increase in the radius of a small aperture by a factor of two could be expected to result in an eight-fold increase in the mutual coupling coefficient. Also, the leakage through small circumferential (transverse) slots is larger than leakage through comparable axial slots since the conduit current is in the axial direction. Therefore, the effect of an extremely narrow transverse slot in a conduit will result in a considerably larger leakage signal than a similar slot in the axial direction.

The induced voltage resulting from an aperture also depends on the location of the internal conductor with respect to the aperture. Furthermore, the diameter and wall thickness of the conduit affect the induced voltages. These factors all influence the amount of magnetic flux linking the internal conductor.

<sup>15</sup>C. G. Montgomery et al., Principles of Microwave Circuits, First Edition (McGraw-Hill, 1948), p 178.

In addition to the magnetic field penetration through openings in a conduit, an electric field which would otherwise terminate on the outer surface of the conduit can penetrate an aperture and terminate on the inner conductor (Figure 29). Thus, besides an inductive coupling component caused by magnetic field coupling, there may also be a capacitive-coupling component resulting from an external electric field normal to the conduit surface in the immediate vicinity of the aperture.

The currents associated with the electric field penetrating to the interior region of a conduit are excited by the conduit potential,  $V_0(t)$ , or the charge density on the outside surface of the conduit. The current induced in the inner conductor by the external electric field penetrating an aperture and terminating on the inner conductor can be represented by a zero-admittance shunt current source:

$$I(t) = C \frac{dV_0(t)}{dt} \quad [\text{Eq 21}]$$

where  $C$  is the capacitive coupling coefficient and  $V_0(t)$  is the voltage between the internal conductor and the conduit.

AMBIENT ELECTRIC FIELD LINES

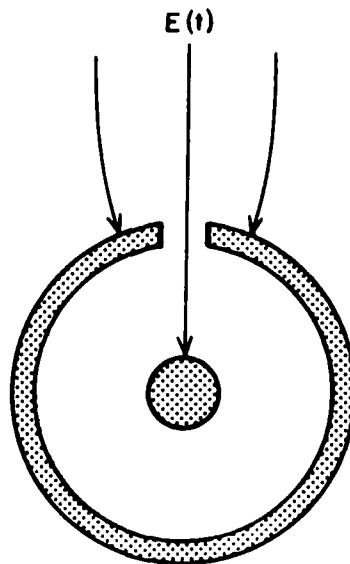


Figure 29. Electric field penetration through an aperture.

Since this external voltage (electric field) mechanism induces a current in the inner conductor, a transfer admittance (as opposed to an impedance) is the appropriate parameter in the frequency domain. In the frequency domain:

$$i(\omega) = -j\omega Cv(\omega) \quad [\text{Eq 22}]$$

where  $i(\omega)$  and  $v(\omega)$  are frequency functions of the current and voltage respectively. The transfer admittance is  $Y = j\omega C$ .

The capacitive coupling coefficient depends on a number of factors, including the electric polarizability,  $p$ , which is a function of the size and shape of the aperture, as shown in Table 13.

Except for very large apertures, the electric field penetration can be expected to be negligible compared with the magnetic field penetration.

### Circuit Model for Leakage-Induced Signals

In the analysis above, the leakage signals induced on an internal conductor caused by current flowing on the exterior of a conduit can be represented by a zero-impedance series voltage source, a zero-admittance shunt current source, or a combination of both. An equivalent circuit model forms the basis of the leakage model described below. This model represents the leakage by an appropriate source at a point on the coaxial line formed by the conduit and the inner conductor.

#### *Source Model*

In this circuit model for EMP leakage, equivalent series voltage and shunt current sources represent the voltages and currents induced on the inner conductor as a result of currents flowing on the outer surface of the conduit. Electromagnetic field leakage through apertures (such as seams, cracks, or openings in a coaxial line) which are caused by current flowing on the exterior in the positive  $z$ -direction can be represented by a zero-impedance series voltage source,  $V_S$ , and a zero-admittance, shunt-current source,  $I_S$ , on a coaxial line of characteristic impedance  $Z_0$  (Figure 30).

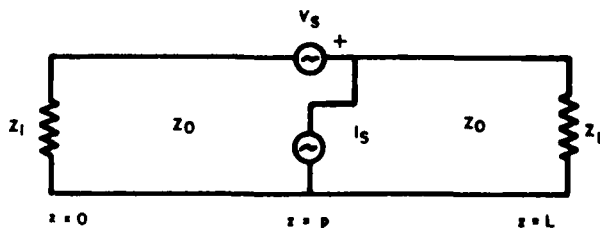


Figure 30. Representative of leakage sources in a coaxial line.

Table 13

Values of the Polarization of Small Holes in Thin Conducting Sheets\*

	$m_1$	$m_2$	$p$
Circle of radius $r$	$\frac{4}{3} r^3$	$\frac{4}{3} r^3$	$\frac{2}{3} r^3$
Ellipse** of eccentricity $\epsilon = \sqrt{1 - \left(\frac{b}{a}\right)^2}$	$\frac{\pi}{3} \frac{ab^2 \epsilon^2}{3(1-\epsilon^2)(F-E)}$	$\frac{\epsilon}{3} \frac{ab^2 \epsilon^2}{E-(1-\epsilon^2)F}$	$\frac{\pi}{3} \frac{ab^2}{E}$
Long narrow ellipse ( $a \gg b$ )	$\frac{\pi}{3} \frac{a^3}{\ln \frac{4a}{b} - 1}$	$\frac{\pi}{3} ab^2$	$\frac{\pi}{3} ab^2$
Slit $c$ of width $d$ and length $l$		$\frac{\pi}{16} l d^2$	$\frac{\pi}{16} l d^2$

\* From C. G. Montgomery et al., Principles of Microwave Circuits, First Edition (McGraw-Hill, 1948), p 178.

\*\*F and E are the complete elliptic integrals of the first and second kinds, respectively:

$$F(\epsilon) = \int_0^{\pi/2} \frac{d\phi}{\sqrt{1-\epsilon^2 \sin^2 \phi}}$$

$$E(\epsilon) = \int_0^{\pi/2} d\phi \sqrt{1-\epsilon^2 \sin^2 \phi}$$

where  $\phi$  is an integration variable.

These integrals are evaluated in Milton Abramowitz and Irene Stegun, eds., Handbook of Mathematical Functions With Formulas, Graphs and Mathematical Tables (U.S. Government Printing Office, May 1968), Table 17.1.

The polarizability  $m_1$  is for the magnetic field parallel to the major semi-axis  $a$ ;  $m_2$  is for the field parallel to the minor semi-axis  $b$ . The magnetic field is transverse to the slit and constant along the length.

The equivalent voltage generator caused by series impedance is in series with the voltage generator for coupling through apertures. Therefore, the complete equivalent voltage source with zero internal impedance is:

$$V_s(t) = RI(t) + M \frac{di}{dt} \quad [\text{Eq 23}]$$

where  $R$  and  $M$  are the resistive coupling coefficient and the mutual inductance coupling coefficient, respectively. Some of these values have been measured experimentally; others can be estimated from flaw impedances and other experimental data. Thus, the defect equivalent voltage source can have a component proportional to the current flowing on the outer surface of the conduit and a component proportional to the time derivation of that current.

As noted earlier, the electric polarizability and the capacitive coupling component are often negligible, except for very large apertures (p 56). Experimental data and interpretation based on the leakage model indicate that the equivalent shunt-current source contribution caused by the capacitive coupling component is small compared with the inductive coupling component for most practical situations. Thus, to simplify the analysis, the current source can be neglected and the leakage effect can be represented entirely by an equivalent voltage source (Figure 31).

Regardless of the exact nature of its origin, the leakage signal can be described to a first approximation by a general model in which the driving voltage induced by a defect has a waveshape that is proportional to the applied conduit current plus its time derivative. The general model for the signals induced by the conduit current,  $I_c(t)$ , caused by a defect is thus:

$$V_d(t) = R_d I_c(t) + M_d \frac{dI_c(t)}{dt} \quad [\text{Eq 24}]$$

where  $R_d$  is a resistive coupling coefficient representing the contribution of a resistive element and  $M_d$  is an inductive coupling coefficient representing the contribution of inductive impedance and coupling between the internal conductor and the magnetic field through an aperture. This simple representation can be used to model most of the observed results of injected current tests.

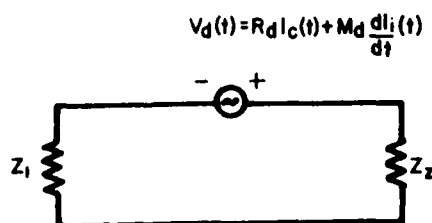


Figure 31. Equivalent circuit without current source.

(Note that this general defect model neglects the direct electric field contribution as discussed above [p 55] and possible effects caused by arcing.)

In the general defect model, both  $R_d$  and  $M_d$  are regarded as constants for a given configuration. Accordingly, each configuration can be assigned a value for each coefficient  $R_d$ (ohms) and  $M_d$ (henries). The coefficient  $M_d$  includes magnetic field coupling through apertures and inductive impedance effects. The value of  $M_d$  for an aperture is determined by all the previously discussed factors, such as the proximity of the internal conductor to the defect, the dimensions of the defect, and the orientation of the defect with respect to the magnetic flux lines.

For the general defect model, with a purely resistive element, the leakage will have the same waveform as the imposed conduit current. Thus, for a simple exponential, the leakage current will also be an exponential, and waveform will be identical to that of the conduit current. For all other transient cases, the waveform will be different from that of the imposed current. In particular, the induced voltage can have a significantly faster rise time than conduit current caused by the  $di/dt$  term. Also, a small but rapidly changing current can induce a large voltage via the inductive components.

For a double exponential form for the conduit current:

$$I_c(t) = I_0 (e^{-t/\tau_1} - e^{-t/\tau_2}) \quad [\text{Eq 25}]$$

where  $\tau_1$  and  $\tau_2$  are the rise time and fall time constants; the time rate of change of the current in amperes per second is:

$$\frac{dI_c(t)}{dt} = I_0 \left( -\frac{1}{\tau_1} e^{-t/\tau_1} + \frac{1}{\tau_2} e^{-t/\tau_2} \right) \quad [\text{Eq 26}]$$

The maximum time rate of change of the conduit current in amperes per second occurs at  $t$  equals 0 and is given by:

$$\frac{dI_c(0)}{dt} = I_0 \frac{\tau_2 - \tau_1}{\tau_1 \tau_2} \quad [\text{Eq 27}]$$

The maximum contribution of the inductive component is, therefore,

$$M \frac{dI_c(0)}{dt} = M I_0 \frac{\tau_2 - \tau_1}{\tau_1 \tau_2} \quad [\text{Eq 28}]$$

A minimum rate of change occurs when the current passes through its maximum value. At this point:

$$\frac{dI_c(t_p)}{dt} = 0 = I_0 \left( -\frac{1}{\tau_1} e^{-t_p/\tau_1} + \frac{1}{\tau_2} e^{-t_p/\tau_2} \right) \quad [\text{Eq 29}]$$

Thus,

$$t_p = \frac{\tau_1 \tau_2}{\tau_2 - \tau_1} \ln \left( \frac{\tau_2}{\tau_1} \right) \quad [\text{Eq 30}]$$

where  $t_p$  is the time of peak conduit current.

The induced voltage source for a double exponential conduit current is:

$$V(t) = R_d I_0 \left[ \left( 1 - \frac{M_d}{R_d \tau_1} \right) e^{-t/\tau_1} - \left( 1 - \frac{M_d}{R_d \tau_2} \right) e^{-t/\tau_2} \right] \quad [\text{Eq 31}]$$

At low frequencies, the resistive component predominates; therefore, the total impedance approaches a constant value about equal to the dc resistance of the defect. At high frequencies, however, the inductive component predominates and the impedance varies linearly with frequency.

#### *Effects of Circuit Configuration*

In the leakage model, a defect is modeled by a voltage source driving the coaxial line formed by the conduit and internal conductor. The induced voltage and the current on the inner conductor depend on the voltage induced onto the inner conductor at the site of the defect, the propagation characteristics of the transmission line formed by the conduit and inner conductor, and the termination impedances at each end.

The analysis of pulse propagation along a transmission line is more complicated than the analysis of time-harmonic propagation because a pulse consists of a spectrum of frequencies which, in general, have different propagation characteristics along the line and different reflection coefficients at the terminations. Qualitatively, the process can be described as follows: at time  $t = 0$ , a voltage pulse is induced at point  $x = x_d$  (Figure 32), and a voltage pulse then propagates toward each end of the conduit with a velocity of propagation  $v$ . When the pulse reaches the end of the line nearer the defect (assumed to be  $x = 0$  for this discussion) at a time  $t = x_d/v$ , the pulse is reflected and propagates in the reverse direction; it is later reflected at  $x = \ell$  (the other end of the conduit-conductor transmission line). Similarly, the pulse propagating toward  $x = \ell$  is reflected and arrives at  $x = 0$  at time  $t = (2\ell - x_d)/v$  where it is also reflected. Thereafter, every  $2\ell/v$  seconds after the arrival of the pulse from either direction, another pulse arrives from the same direction. The magnitude and waveform of the reflected pulses depend on the propagation and attenuation characteristics of the line and the terminations at each end. A detailed analysis of pulse propagation on transmission lines is given by G. Metzger and J. P. Valore.<sup>16</sup>

<sup>16</sup>G. Metzger and J. P. Valore, Transmission Lines With Pulse Excitation (Academic Press, 1969).

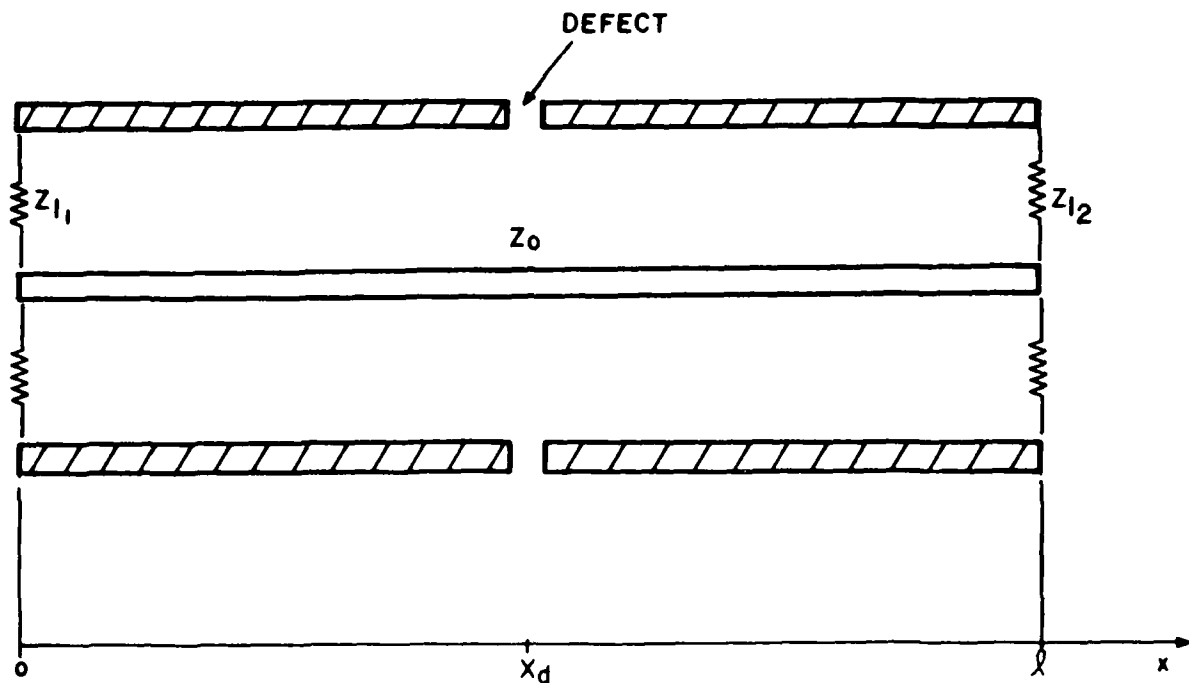


Figure 32. Coaxial transmission line.

For a concentric coaxial transmission line, the high-frequency inductance per unit length is:

$$L = \frac{\mu_0}{2\pi} \ln(b/a) \text{ henries/meter } (= 3.28 \frac{\mu_0}{2\pi} \ln(\frac{b}{a}) \text{ henries/ft}) \quad [\text{Eq 32}]$$

where  $a$  = inner conductor radius  
 $b$  = outer conductor radius  
 $\mu_0$  = permeability of the dielectric.

The capacitance per unit length is:

$$C = \frac{2\pi\epsilon}{\ln(b/a)} \text{ farads/meter } = \frac{6.6\pi\epsilon}{\ln(b/a)} \text{ farads/foot} \quad [\text{Eq 33}]$$

where  $\epsilon$  equals the dielectric constant of the insulating material.

The characteristic impedance for a transmission line is:

$$Z_0 = \sqrt{\frac{j\omega L_\ell + R_\ell}{j\omega C_\ell + G_\ell}} \quad [\text{Eq 34}]$$

where  $\omega$  = the radian frequency =  $2\pi f$   
 $G$  = the conductance of the line.

For a lossless line, the characteristic impedance is:

$$Z_0 = \sqrt{\frac{L_\ell}{C_\ell}} = \frac{1}{2\pi} \sqrt{\frac{\mu}{\epsilon}} \ln(b/a) \quad [\text{Eq 35}]$$

If an end is terminated in the characteristic impedance, there is no reflection. If an end is short-circuited, its reflection coefficient is -1; if an end is open-circuited, its reflection coefficient is +1.

At the low frequency limit, the transmission line can be represented by lumped circuit elements. That is, the voltage appearing at the defect drives a resistor and an inductor in series (Figure 33). This situation is described by:

$$L_s \frac{dI(t)}{dt} + R_s I(t) = V_d(t) \quad [\text{Eq 36}]$$

where  $L_s$  is the series inductance,  $R_s$  is the series resistance, and  $V_d(t)$  is the voltage resulting from by the defect. With the condition that  $I(0) = 0$ , the solution to this equation is:

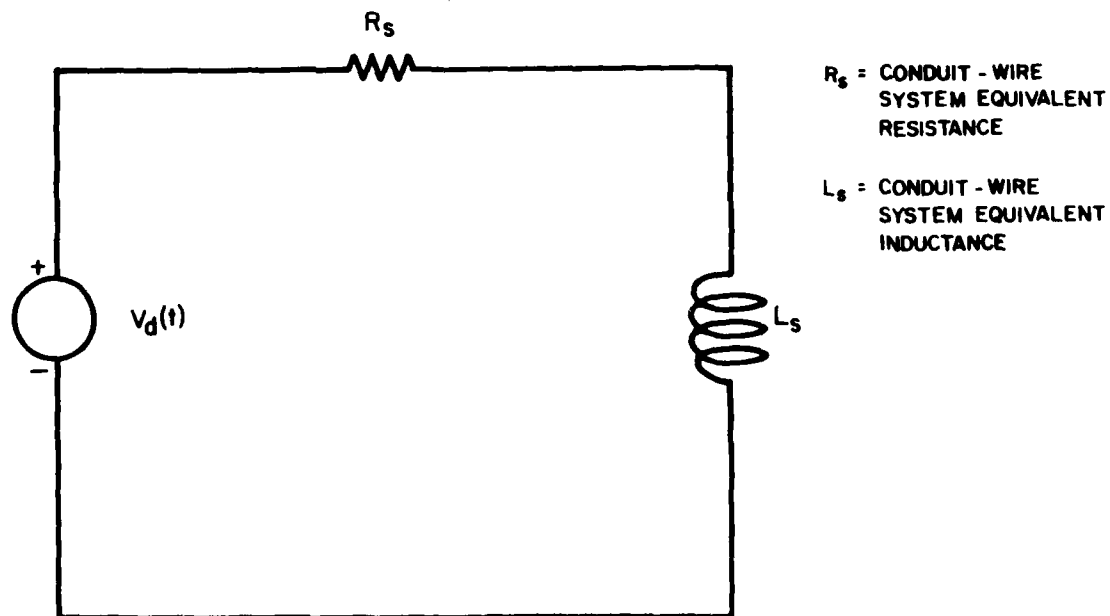


Figure 33. Equivalent lumped parameter circuit.

$$I(t) = \frac{e^{-\frac{R_s}{L_s} t}}{L_s} \int_0^t V_d(t) e^{\frac{R_s}{L_s} t} dt \quad [\text{Eq 37}]$$

For a transmission line, the total resistance and the total inductance are proportional to the length of the line. Thus, in the case of a transmission line short-circuited at both ends, and with no additional resistance or inductance, the ratio  $R_s/L_s$  is independent of length (i.e., it is the constant  $R_\ell/L_\ell$  for a particular transmission line configuration), and the short-circuit current is inversely proportional to the length:

$$I(t) = \frac{e^{-\frac{R_\ell}{L_\ell} t}}{L_\ell} \int_0^t V_d(t) e^{\frac{R_\ell}{L_\ell} t} dt \quad [\text{Eq 38}]$$

Substitution of the circuit model for the series voltage generator given earlier (p 56) yields the following relation for the inner conductor current in terms of the conduit current:

$$I(t) = \frac{M_d}{L} (I_c(t) - I_c(0) e^{-\frac{R}{L} t}) \quad [\text{Eq 39}]$$

$$+ \frac{R}{L} \left( \frac{R_d}{R} - \frac{M_d}{L} \right) e^{-\frac{R}{L} t} \int_0^t e^{\frac{R}{L} t} I_c(t) dt$$

For the double exponential waveform:

$$I(t) = I_0 (e^{-\frac{t}{\tau_1}} - e^{-\frac{t}{\tau_2}}), \quad [\text{Eq 40}]$$

$$I(t) = I_0 \left\{ - \frac{\left( \frac{\tau_c}{\tau_2} - \frac{\tau_c}{\tau_1} \right) \left( \frac{R_d}{R} - \frac{M_d}{L} \right)}{\left( 1 - \frac{\tau_c}{\tau_1} \right) \left( 1 - \frac{\tau_c}{\tau_2} \right)} e^{-\frac{t}{\tau_c}} \right.$$

$$+ \left[ \frac{M_d}{L} + \left( \frac{R_d}{R} - \frac{M_d}{L} \right) \frac{1}{\left( 1 - \frac{\tau_c}{\tau_1} \right)} \right] e^{-\frac{t}{\tau_1}}$$

$$\left. - \left[ \frac{M_d}{L} + \left( \frac{R_d}{R} - \frac{M_d}{L} \right) \frac{1}{\left( 1 - \frac{\tau_c}{\tau_2} \right)} \right] e^{-\frac{t}{\tau_2}} \right\}$$

where  $\tau_c = \frac{L}{R}$  is a time constant associated with the lumped parameter L-R circuit (Figure 33).

The reflections from the ends of an electrically short transmission line terminated in short circuits at both ends will result in a buildup of current (Figure 34). A similar voltage buildup will occur on open circuits that are electrically short.

#### Coupling Coefficients ( $R_d$ and $M_d$ ) From Flaw Impedances

Values for leakage current coupling coefficients can be determined from flaw impedance plots presented by the Harry Diamond Laboratories.<sup>17</sup> Examples

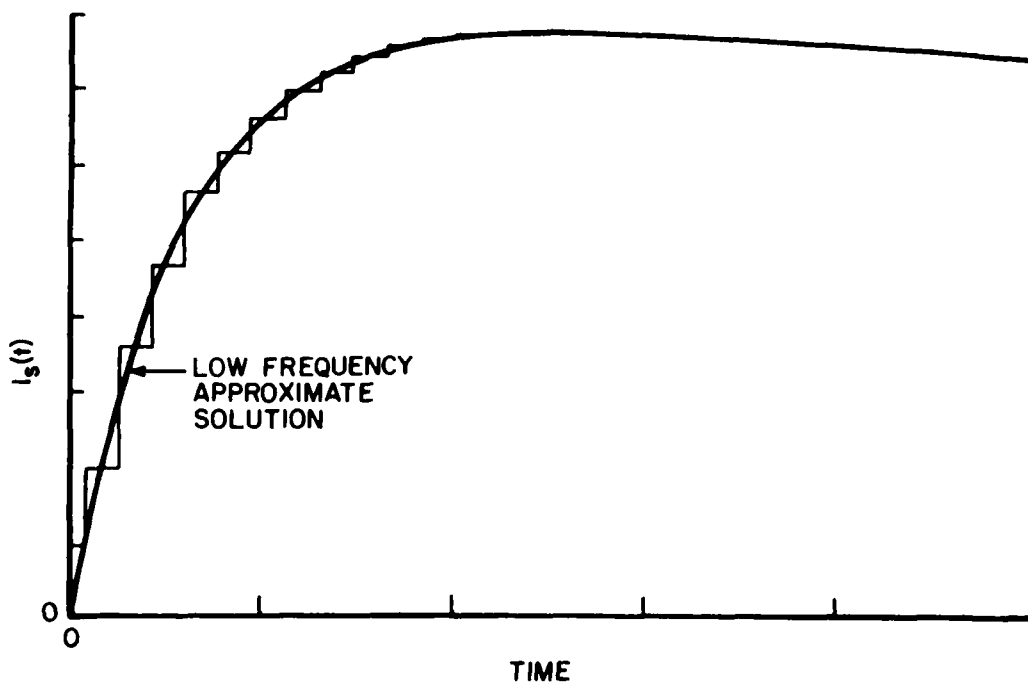


Figure 34. Buildup of short-circuit current.

<sup>17</sup>H. A. Roberts and J. Capobianco, Safeguard Buried Conduit Studies, HDL-TR-1850 (Harry Diamond Laboratories, September 1978).

of these are Figure 1 (conduit coupling), Figure 2 (conduit union), and Figure 8 (large aperture). The plots given are  $20 \log (1 Z_F 1/2 Z_0)$  versus frequency. A value for  $R_d$  is found from the lowest frequency value plotted (approximating the dc value), and a value for  $M_d$  is found for the highest-frequency plotted value.

$$R_d = 200 \times 10^{-Z_{LF}/20} \quad [\text{Eq 41}]$$

and

$$M_d = 200 \times 10^{-Z_{HF}/20}$$

where  $Z_{LF}$  = the low frequency value (in dB read from the plot)

$Z_{HF}$  = the high frequency value  
= the radian frequency =  $2 f$ , where  $f$  is the frequency in Hertz.

The following coupling coefficients have been determined from the Harry Diamond Laboratories' plots:

1. Rusted coupling (Figure 1).

$$R_d = 1.12 \times 10^{-1}$$

$$M_d = 1.267 \times 10^{-9}$$

2. Transverse slot in 4-in. (102.6-mm) inner diameter conduit, width equals 1.2 in. (12.7 mm) length equals 7 in. (177.8 mm) (wire in center).

$$R_d = 1.78 \times 10^{-4}$$

$$M_d = 7.13 \times 10^{-10}$$

3. Transverse slot (same as 2) with wire in three different locations.

- a. Near slot:

$$R_d = 1.12 \times 10^{-3}$$

$$M_d = 5.05 \times 10^{-9}$$

- b. Center:

$$R_d = 1.59 \times 10^{-4}$$

$$M_d = 6.37 \times 10^{-10}$$

- c. Opposite slot:

$$R_d = \text{indeterminate, smaller than } 1.5 \times 10^{-5}$$

$$M_d = 5.67 \times 10^{-11}$$

4. Large aperture (Figure 8).

$$R_d = 2.24 \times 10^{-2}$$

$$M_d = 1.42 \times 10^{-7}$$

5. Conduit union (Figure 2).

a. Case I:

$$R_d = 4.48 \times 10^{-4}$$

$$M_d = 7.99 \times 10^{-11}$$

b. Case II:

$$R_d = 1.26 \times 10^{-4}$$

$$M_d = 1.01 \times 10^{-11}$$

c. Case III: not calculated

d. Case IV:

$$R_d = 1.42 \times 10^{-3}$$

$$M_d = 1.27 \times 10^{-9}$$

e. Case V:

$$R_d = 6.32 \times 10^{-4}$$

$$M_d = 1.59 \times 10^{-10}$$

## 7 CONCLUSIONS

This report has presented the results of CERL's study to develop shielding tests and design criteria for EMP/EMI hardened conduit systems. Included were: (1) an evaluation of conduit hardware characteristics, (2) development of special EMP conduit hardware items, (3) an evaluation of "in situ" conduit system test techniques, and (4) development of analytic techniques for EMP hardness assessment of conduit systems.

1. EMP signals can be transferred to conductors inside conduits by diffusion through the conduit wall or by a number of leakage coupling mechanisms, the most important of which are resistive and inductive. Pulse signals resulting from diffusion have significantly lower high-frequency content than those resulting from the leakage coupling mechanisms, and present the maximum shielding that can be obtained from a conduit.

2. The principles discussed above were applied for development of EMP hardened conduit hardware items. These included an experimental, EMP-resistant union designed to allow a considerable angular offset, a case-access fitting cover, and a junction box cover. While these items provided an increase in EMP hardness, their cost effectiveness will have to be decided by individual analysis.

3. Three "in situ" test techniques were evaluated. Each concept was found effective in locating conduit defects; each, however, has some limitations. The Hall effect and S-band resonant cavity techniques require both access to suspected defect locations and a separate test fixture for each conduit size. The standing-wave technique requires two or more parallel conduits. Even with these limitations, the techniques should find some application for defect determination and location.

4. The analytic techniques for hardness assessment of conduit systems include a diffusion current analysis and a leakage current analysis. The diffusion current analysis is based on the impulse response of a cylindrical structure. The accuracy to which the diffusion waveshape can be determined is essentially limited only by the accuracy of the determination of the EMP current waveform on the conduit and by the material properties of that conduit. The diffusion current analysis is useful for determining wall thickness and materials required for conduit systems. In addition, this analysis can check the EMP hardness provided by existing systems or specific items, such as flexible conduits, with fixed wall thicknesses. The leakage current analysis uses individual item "coupling coefficients," both resistive and inductive. The accuracy of the prediction of leakage current is, of course, dependent on the accuracy of the values for these coefficients. The leakage current analysis is useful mainly for assessing the EMP hardening provided by conduit hardware items with threads, possible apertures, and mating surfaces.

As a result of this study, CERL developed five design criteria for EMP/EMI hardened conduit systems:

1. For control of diffusion current levels, rigid steel conduit is generally satisfactory; however, a hardness assessment should be performed to confirm this. The assessment should take into account the proposed conduit

system's material properties, including electrical conductivity, magnetic permeability, and physical dimensions.

2. Leakage can be reduced by adequately tightening joints, eliminating apertures, and using designs with well-matched, low-resistance mating surfaces.

3. The surface resistance of the mating parts can often be reduced by coating the surfaces with a material such as zinc or tin, which forms a soft, low-resistance, contact surface.

4. Flame-spraying techniques appear to provide good adhesion to metallic surfaces and are satisfactory for this application.

5. Unassembled conduit threads must be protected from rust and corrosion to prevent unnecessary resistance in the conduit system.

## REFERENCES

- Abramowitz, Milton and Irene Stegun, eds., Handbook of Mathematical Functions With Formulas, Graphs and Mathematical Tables (U.S. Government Printing Office, May 1968).
- Croissant, W., P. Nielsen, D. Sieber, and R. G. McCormack, Development of a Conduit Design Analytical Procedure, Interim Report M-234/ADA056218 (U.S. Army Construction Engineering Research Laboratory [CERL], June 1978).
- Electronics Engineers Handbook (McGraw-Hill Book Company, 1975).
- Leverenz, D. J., R. G. McCormack, P. H. Nielsen, Development and Evaluation of Repairs for EMP Leaks in Conduit Systems, Technical Report C-17/ADA011223 (CERL, April 1975).
- Leverenz, D. J., R. G. McCormack, and P. H. Nielsen, EMP Shielding Properties of Conduit Systems and Related Hardware, Technical Report C-19/ADA012729 (CERL, June 1975).
- Leverenz, D. J., R. G. McCormack, P. H. Nielsen, EMP Evaluation of Junction Boxes, Junction Box Covers, and Gaskets, Technical Report C-18/ADA010631 (CERL, May 1975).
- Metzer, G. and J. P. Valore, Transmission Lines With Pulse Excitation (Academic Press, 1969).
- Montgomery, C. G. et al., Principles of Microwave Circuits, First Edition (McGraw-Hill, 1948), p 178.
- Reference Data for Radio Engineers, Sixth Edition (Howard W. Sams & Co., Inc., 1975).
- Roberts, H. A. and J. Capobianco, Safeguard Buried Conduit Studies, HDL-TR-1850 (Harry Diamond Laboratories, September 1978).
- Whitson, A. L. and E. F. Vance, Bolt Lapped-Joint EMP Shields, DNA 4472-F (Defense Nuclear Agency, June 1977).
- Underwriters Laboratories, Inc., Revision of the Outline of the Proposed Investigation for Intermediate Metal Conduit (May 24, 1977).
- Underwriters Laboratories Inc., Standard for Electrical Metallic Tubing, Fourth Edition, Standard 797 (August 19, 1977).

APPENDIX:

EXAMPLE PROBLEMS -- DIFFUSION AND LEAKAGE CURRENT ANALYSES

Diffusion Current

*Sample Problem*

A facility consisting of two shielded zones 400 m apart is planned. The design calls for the shielded zones to be joined with a 1-in. rigid steel conduit carrying a number of conductors, one of which is a 12-gauge wire with low impedance terminations (essentially short circuits). The design conduit current for this problem is a double exponential with a peak magnitude of 2000 A and time constants  $\tau_1 = 6.7 \times 10^{-7}$  seconds and  $\tau_2 = 3.8 \times 10^{-9}$  seconds or:

$$I(t) = I_0 \left( e^{-\frac{t}{\tau_1}} - e^{-\frac{t}{\tau_2}} \right) = 2000 \left( e^{-\frac{t}{6.7 \times 10^{-7}}} - e^{-\frac{t}{3.8 \times 10^{-9}}} \right) \quad [\text{Eq A1}]$$

The problem is determining the diffusion current magnitude and the time of occurrence of the peak magnitude.

*Diffusion Current Calculations*

The calculations are done according to the following steps:

1. Determine the physical properties (conductivity, permeability, dimensions) of the conduit system.
2. Estimate the charge transported by the conduit current.
3. Calculate the diffusion time constant.
4. Determine the peak value of open-circuit voltage (this is necessary for the later determination of the short-circuit current).
5. Determine the wire-conduit parameters (resistance and inductance).
6. Determine short-circuit current amplitude.

1. Physical Properties of the Conduit.

For greatest accuracy, the conductivity and permeability of the conduit should be measured; since these parameters are not subject to control, they are somewhat variable; however, for most calculations, the values from the tables in Chapter 5 should be adequate. For this example, values of  $7.2 \times 10^6$  mho/m (Table 6) conductivity and  $130 \times 4 \times 10^{-7}$  henries/m (an experimentally

determined value) for permeability are used.<sup>18</sup> The conduit length is 400 m and the wall thickness for a 1-in. rigid steel conduit is 3.38 mm (Table 7).

## 2. Charge Transported.

The charge transported is:

$$I = \frac{dQ}{dt} \text{ or } dQ = Idt \text{ and } Q = \int_0^{\infty} Idt \quad [\text{Eq A2}]$$

or

$$Q = \int_0^{\infty} Idt = \int_0^{\infty} I_0 (e^{-\tau_1 t} - e^{-\tau_2 t}) dt = I_0 (e^{-\tau_1 t} - e^{-\tau_2 t})$$

$$= 2000 \left( e^{-\frac{t}{6.7 \times 10^{-7}}} - e^{-\frac{t}{3.8 \times 10^{-9}}} \right)$$

where  $I_0 = 2000$ ,  $\tau_1 = 6.7 \times 10^{-7}$  seconds, and  $\tau_2 = 3.8 \times 10^{-9}$  seconds (the amplitude and waveshape specified in the problem). The calculation gives:

$$I_0(\tau_1 - \tau_2) = 2 \times 10^3(6.7 \times 10^{-7} - 3.8 \times 10^{-9}) = 0.17 \times 10^{-2} \text{ coulomb} \quad [\text{Eq A3}]$$

## 3. Diffusion Time Constant.

The formula for the diffusion time constant is:

$$T = \frac{\mu\sigma(b-a)^2}{4} \quad [\text{Eq A4}]$$

where  $b - a$  is the conduit thickness,  $\mu$  (permeability) =  $130 \times 4 \times 10^{-7}$  henries/m, and  $\sigma$  (conductivity) =  $7.2 \times 10^{-6}$  = mho/m. Therefore,

$$\frac{(b-a)^2}{4} = \frac{4 \times 130 \times 10^{-7} \times 7.2 \times 10^{-6} (3.38 \times 10^{-3})^2}{4} \quad [\text{Eq A5}]$$

$$= 3.36 \text{ milliseconds}$$

The time when the peak occurs is  $0.656 T$  or  $0.656 \times 3.36 \times 10^{-3} = 2.20$  milliseconds.

<sup>18</sup>W. Croisant, P. Nielsen, D. Sieber, and R. G. McCormack, Development of a Conduit Design Analytical Procedure, Interim Report M-234/ADA056218 (CERL, June 1978).

#### 4. Peak Open-Circuit Voltage.

The formula for peak open-circuit voltage is:

$$V_{OC} = 0.656 QF\ell \quad [\text{Eq A6}]$$

where  $Q$  is the previously determined (Step 2, above) charge transported =  $0.17 \times 10^{-2}$  coulomb, and  $\ell$  = the conduit length = 400 m, and

$$F = \frac{8}{\pi^{3/2} \sqrt{ab} \mu \sigma^2 (b-a)^3} \quad [\text{Eq A7}]$$

where  $a$  = inside diameter of the conduit =  $1.33 \times 10^{-2}$  m,  $b$  = outside diameter of the conduit =  $1.67 \times 10^{-2}$  m or:

$$F = \frac{8}{\pi^{3/2} \sqrt{1.67 \times 10^{-2} \times 1.33 \times 10^{-2}} \times 130 \times 4\pi \times 10^{-7}} \quad [\text{Eq A8}]$$
$$\times \frac{1}{(7.2 \times 10^{-6})^2 (1.67 \times 10^2 - 1.33 \times 10^2)} = 0.296$$

and  $V_{OC} = 0.656QF\ell = 0.656 \times 0.17 \times 10^{-2} \times 0.296 \times 400 = 0.132$  V.

#### 5. Wire-Conduit Circuit Parameters.

The resistance for 12-gauge copper wire is  $1.59 \times 10^{-3}$  ohm/ft (from Table 10) or 2.09 ohms for 400 m. The conduit resistance is  $4.1 \times 10^{-4}$  ohm/m (Table 11) or  $16.4 \times 10^{-2}$  ohms for 400 m. The total resistance for the wire-conduit circuit is  $2.09 + 16.4 \times 10^{-2} = 2.25$  ohms. The high-frequency inductance for a 12-gauge wire inside a 1-in. conduit is  $5.15 \times 10^{-7}$  henries/m (Table 12), or a total inductance of  $2.06 \times 10^{-4}$  henries.

#### 6. Short-Circuit Current Amplitude.

To determine the short-circuit current, it is necessary to find the peak amplitude factor by calculating  $\alpha = TR/L$  and reading the peak amplitude factor from either the graph or table on Figure 27.  $T$  is the previously determined diffusion time constant, and  $R$  and  $L$  are the wire-conduit circuit values of resistance and inductance found in Step 5 above.

For this problem  $\alpha = 3.36 \times 10^{-3} \times 2.25 : 2.06 \times 10^{-4} = 3.69$  second-ohm/m; the peak amplitude factor = 0.02. The short-circuit current is determined from the formula

$$I_{SC} = \frac{1.351 V_{OC} T}{L} \times \text{peak amplitude factor} \quad [\text{Eq A9}]$$

where  $V_{OC}$  has been determined in Step 4 above as 0.132 V, where  $T = 3.36$  milliseconds from Step 3 above.  $L = 2.06 \times 10^{-4}$  henries from Step 5 above:

$$I_{SC} = \frac{1.351 \times 0.132 \times 3.36 \times 10^{-3} \times 0.02}{2.06 \times 10^{-4}} = 58 \text{ milliamperes [Eq A10]}$$

This is the peak value of the short-circuit current, the time when the peak occurs (Step 3 above) is 2.20 milliseconds.

#### Leakage Current From a Defect Sample Problem

A defect with  $R_d = 0.01$  ohm and  $M_d = 1 \times 10^{-10}$  henries exists 80 m from the far end of the conduit system described in the previous example. This defect is representative of the resistance of a clean coupling installed on rusty conduit threads. The coupling coefficient  $M_d$  may be representative of a cracked coupling or a leaky union, i.e., a defect with no large open areas.

The excitation waveform is the same as that described in the previous example, i.e., a double exponential with  $I_0 = 2000$  A:

$$\tau_1 = 6.7 \times 10^{-7} \text{ seconds}$$

$$\tau_2 = 3.8 \times 10^{-9} \text{ seconds}$$

It is necessary to determine the current pulse at a short-circuit termination at the near end of the conduit (320 m from the defect). Eq 40 is used to obtain an estimate of the short-circuit current caused by such a defect:

$$I(t) = I_0 \left\{ \frac{\left( \frac{\tau_c}{\tau_2} - \frac{\tau_c}{\tau_1} \right) \left( \frac{R_d}{R} - \frac{M_d}{L} \right) - \frac{t}{\tau_c}}{\left( 1 - \frac{\tau_c}{\tau_1} \right) \left( 1 - \frac{\tau_c}{\tau_2} \right)} e^{-\frac{t}{\tau_c}} \right. \quad \text{[Eq A 11]} \\ \left. + \left[ \frac{M_d}{L} + \left( \frac{R_d}{R} - \frac{M_d}{L} \right) \frac{1}{\left( 1 - \frac{\tau_c}{\tau_1} \right)} \right] e^{-\frac{t}{\tau_1}} \right. \\ \left. - \left[ \frac{M_d}{L} + \left( \frac{R_d}{R} - \frac{M_d}{L} \right) \frac{1}{\left( 1 - \frac{\tau_c}{\tau_2} \right)} \right] e^{-\frac{t}{\tau_2}} \right\}$$

From the first example, R was found to be 2.25 ohms. (Conduit resistance from Table 11 and wire resistance from Table 10.) The inductance (from Table 12) was found to be  $2.06 \times 10^{-4}$  henries:

$$\tau_c = L/R = 9.16 \times 10^{-5} \text{ seconds} = 91.6 \text{ microseconds} \quad [\text{Eq A12}]$$

Thus,

$$\frac{\tau_c}{\tau_1} = \frac{9.16 \times 10^{-5} \text{ sec}}{6.7 \times 10^{-7} \text{ sec}} = 1.37 \times 10^2$$

$$\frac{\tau_c}{\tau_2} = \frac{9.16 \times 10^{-5}}{3.8 \times 10^{-9}} = 2.41 \times 10^4$$

$$\frac{R_d}{R} = \frac{0.01}{2.25} = 4.44 \times 10^{-3}$$

$$\frac{M_d}{L} = 4.85 \times 10^{-7}$$

$$\frac{R_d}{R} - \frac{M_d}{L} = 4.44 \times 10^{-3}$$

resulting in:

$$I(t) = 2000 \left[ 3.25 \times 10^{-5} e^{-\frac{t}{9.16 \times 10^{-5}}} + 3.22 \times 10^{-5} e^{-\frac{t}{6.7 \times 10^{-5} \text{ sec}}} - 3.01 \times 10^{-7} e^{-\frac{t}{3.8 \times 10^{-9} \text{ sec}}} \right]$$

For this example, the conduit current pulse duration is short with respect to the propagation time along the length of the conduit. Thus, current adding effects will not occur. (An estimate for propagation velocity is 1 nanosecond/ft or slightly more than 3 nanoseconds/m.) End-to-end propagation time for a 400-m conduit is thus approximately 1.5 microseconds; the driving pulse will be over when the reflections occur.

CERL DISTRIBUTION

Chief of Engineers  
 ATTN: Tech Monitor  
 ATTN: DAEN-ASI-L (2)  
 ATTN: DAEN-CCP  
 ATTN: DAEN-CW  
 ATTN: DAEN-CWE  
 ATTN: DAEN-CWM-R  
 ATTN: DAEN-CWO  
 ATTN: DAEN-CWP  
 ATTN: DAEN-MP  
 ATTN: DAEN-MPC  
 ATTN: DAEN-MPE  
 ATTN: DAEN-MPG  
 ATTN: DAEN-MPR-A  
 ATTN: DAEN-RD  
 ATTN: DAEN-RDC  
 ATTN: DAEN-RDM  
 ATTN: DAEN-RM  
 ATTN: DAEN-ZC  
 ATTN: DAEN-ZCE  
 ATTN: DAEN-ZCI  
 ATTN: DAEN-ZCM

US Army Engineer Districts

ATTN: Library  
 Alaska  
 Al Batin  
 Albuquerque  
 Baltimore  
 Buffalo  
 Charleston  
 Chicago  
 Detroit  
 Far East  
 Fort Worth  
 Galveston  
 Huntington  
 Jacksonville  
 Japan  
 Kansas City  
 Little Rock  
 Los Angeles  
 Louisville  
 Memphis  
 Mobile  
 Nashville  
 New Orleans  
 New York  
 Norfolk  
 Omaha  
 Philadelphia  
 Pittsburgh  
 Portland  
 Riyadh  
 Rock Island  
 Sacramento  
 San Francisco  
 Savannah  
 Seattle  
 St. Louis  
 St. Paul  
 Tulsa  
 Vicksburg  
 Walla Walla  
 Wilmington

US Army Engineer Divisions

ATTN: Library  
 Europe  
 Huntsville  
 Lower Mississippi Valley  
 Middle East  
 Middle East (Rear)  
 Missouri River  
 New England  
 North Atlantic  
 North Central  
 North Pacific  
 Ohio River  
 Pacific Ocean  
 South Atlantic  
 South Pacific  
 Southwestern

Waterways Experiment Station  
 ATTN: Library

Cold Regions Research Engineering Lab  
 ATTN: Library

US Government Printing Office  
 Receiving Section/Depository Copies (2)

Defense Technical Information Center  
 ATTN: DDA (12)

Engineering Societies Library  
 New York, NY

FESA, ATTN: Library

ETL, ATTN: Library

Engr. Studies Center, ATTN: Library  
 Inst. for Water Res., ATTN: Library

SHAPE  
 ATTN: Survivability Section, CCB-OPS  
 Infrastructure Branch, LANDA

HQ USFUCOM  
 ATTN: ECU 477-LOE

Army Instl. and Major Activities (CONUS)  
 DARCOM - Dir., Instl. & Svcs.

ATTN: Facilities Engineer  
 ARRADCOM  
 Aberdeen Proving Ground  
 Army Matls. and Mechanics Res. Ctr.  
 Corpus Christi Army Depot  
 Harry Diamond Laboratories  
 Dugway Proving Ground  
 Jefferson Proving Ground  
 Fort Monmouth  
 Letterkenny Army Depot  
 Natick Research and Dev. Ctr.  
 New Cumberland Army Depot  
 Pueblo Army Depot  
 Red River Army Depot  
 Redstone Arsenal  
 Rock Island Arsenal  
 Savanna Army Depot  
 Sharpe Army Depot  
 Seneca Army Depot  
 Tobyhanna Army Depot  
 Tooele Army Depot  
 Watervliet Arsenal  
 Yuma Proving Ground  
 White Sands Missile Range

FORSCOM

FORSCOM Engineer, ATTN: AFEN-FE  
 ATTN: Facilities Engineers  
 Fort Buchanan  
 Fort Bragg  
 Fort Campbell  
 Fort Carson  
 Fort Devens  
 Fort Drum  
 Fort Hood  
 Fort Indiantown Gap  
 Fort Irwin  
 Fort Sam Houston  
 Fort Lewis  
 Fort McCoy  
 Fort McPherson  
 Fort George G. Meade  
 Fort Ord  
 Fort Polk  
 Fort Richardson  
 Fort Riley  
 Presidio of San Francisco  
 Fort Sheridan  
 Fort Stewart  
 Fort Wainwright  
 Vancouver Bks.

TRADOC

HQ, TRADOC, ATTN: ATEN-FE  
 ATTN: Facilities Engineer  
 Fort Belvoir  
 Fort Benning  
 Fort Bliss  
 Carlisle Barracks  
 Fort Chaffee  
 Fort Dix  
 Fort Eustis  
 Fort Gordon  
 Fort Hamilton  
 Fort Benjamin Harrison  
 Fort Jackson  
 Fort Knox  
 Fort Leavenworth  
 Fort Lee  
 Fort McClellan  
 Fort Monroe  
 Fort Rucker  
 Fort Sill  
 Fort Leonard Wood  
 INSCOM - Ch. Instl. Div.  
 ATTN: Facilities Engineer  
 Vint Hill Farms Station  
 Arlington Hall Station

WESTCOM

ATTN: Facilities Engineer  
 Fort Shafter

MDW

ATTN: Facilities Engineer  
 Cameron Station  
 Fort Lesley J. McNair  
 Fort Myer

HSC

HQ USAHSC, ATTN: H100  
 T3: Facilities Engineer  
 Fitzsimons Army Medical Center  
 Walter Reed Army Medical Center

USACC

ATTN: Facilities Engineer  
 Fort Huachuca  
 Fort Ritchie

MTMC

HQ, ATTN: MTMC-5A  
 ATTN: Facilities Engineer  
 Oakland Army Base  
 Bayonne M&T  
 Sunny Point M&T

US Military Academy

ATTN: Facilities Engineer  
 ATTN: Dept of Geography &  
 Computer Science  
 ATTN: D44PEP/MAEN-A

USAFES, Fort Belvoir, VA

ATTN: AT/A-20E-1K  
 ATTN: AT/A-20E-1K  
 ATTN: AT/A-20E-1K  
 ATTN: Engr. Library

Chief Inst. Div., JASA, Rock Island, IL

USA ARRCOM, ATTN: Dir., Instl. Svcs.

TARCOM, Fac. Div.

TECOM, ATTN: DR/TECOM

TSARCOM, ATTN: DR/TSARCOM

NARAD COM, ATTN: DR/NARAD

AMMRC, ATTN: DR/AMMRC

HQ, XVIII Airborne Corps and

Ft. Bragg

ATTN: AFZA-FE-EE

HQ, 7th Army Training Command

ATTN: AETTC-DEB (4)

HQ USAREUR and 7th Army

ODCS/Engineer

ATTN: AEAEN-Eh (4)

V Corps

ATTN: AETVDEH (4)

VII Corps

ATTN: AETSDEH (4)

21st Support Command

ATTN: AEREM (4)

US Army Berlin

ATTN: AERA-EN (2)

US Army Southern European Task Force

ATTN: AESE-ENG (5)

US Army Installation Support Activity

Europe

ATTN: AEUES-RP

8th USA, Korea

ATTN: EAPE

Cdr, Fac Engr Act (4)

AFE, Yongsan Area

AFE, 2D Inf Div

AFE, Area II Spt Bct

AFE, Cp Humphreys

AFE, Pusan

AFE, Taegu

DLA ATTN: DLA-WI

USA Japan (USARJ)

Ch, FE Div, AJEN-FE

Fac Engr (Honshu)

Fac Engr (Okinawa)

ROK/US Combined Forces Command

ATTN: EUSA-HHC-CFC/ENR

416th Engineer Command

ATTN: Facilities Engineering

Norton AFB

ATTN: AFRCCE-MX/DEE

Port Hueneke, CA 94043

ATTN: Library (Code LUHA)

AFESC/Engineering & Service Lab

Tyndall AFB, FL 32403

Chanute AFB, IL 61866

3345 CES/DE, Stop 27

National Guard Bureau

Installation Division

WASH DC 20310

+EMS team

Nielsen, Paul H.  
EMP/EMI hardening of electrical conduit systems. -- Champaign, IL :  
Construction Engineering Research Laboratory ; Springfield, VA : available  
from NTIS, 1981.  
74 p. (Technical report ; M-292

1. Electric conduits. 2. Shielding (electricity). I. Title. II. Series:  
U.S. Army. Construction Engineering Research Laboratory. Technical report ;  
M-292.